



Published in final edited form as:

Neuroimage. 2014 June ; 93(Pt 2): 260–275. doi:10.1016/j.neuroimage.2013.05.052.

Cytoarchitecture, probability maps and functions of the human frontal pole

S. Bludau^{a,*}, S.B. Eickhoff^{a,b}, H. Mohlberg^a, S. Caspers^a, A.R. Laird^{c,d,i}, P.T. Fox^{c,d,e}, A. Schleicher^a, K. Zilles^{a,f,g}, and K. Amunts^{a,g,h}

^aResearch Centre Jülich, Institute of Neuroscience and Medicine (INM-1), 52425 Jülich, Germany

^bInstitute for Clinical Neuroscience and Medical Psychology, Heinrich-Heine-University Düsseldorf, 40001 Düsseldorf, Germany

^cResearch Imaging Institute, University of Texas Health Science Center, San Antonio, TX, USA

^dDepartment of Radiology, University of Texas Health Science Center, San Antonio, TX, USA

^eSouth Texas Veterans Health Care System, San Antonio, TX, USA

^fDept. of Psychiatry, Psychotherapy and Psychosomatics, RWTH University Aachen, 52074 Aachen, Germany

^gJARA, Juelich-Aachen Research Alliance, Translational Brain Medicine, Jülich, Germany

^hC. and O. Vogt Institute for Brain Research, Heinrich-Heine-University Düsseldorf, 40001 Düsseldorf, Germany

ⁱDepartment of Physics, Florida International University, Miami, FL, USA

Abstract

The frontal pole has more expanded than any other part in the human brain as compared to our ancestors. It plays an important role for specifically human behavior and cognitive abilities, e.g. action selection (Kovach et al., 2012). Evidence about divergent functions of its medial and lateral part has been provided, both in the healthy brain and in psychiatric disorders. The anatomical correlates of such functional segregation, however, are still unknown due to a lack of stereotaxic, microstructural maps obtained in a representative sample of brains. Here we show that the human frontopolar cortex consists of two cytoarchitectonically and functionally distinct areas: lateral frontopolar area 1 (Fp1) and medial frontopolar area 2 (Fp2). Based on observer-independent mapping in serial, cell-body stained sections of 10 brains, three-dimensional, probabilistic maps of areas Fp1 and Fp2 were created. They show, for each position of the reference space, the probability with which each area was found in a particular voxel. Applying these maps as seed regions for a meta-analysis revealed that Fp1 and Fp2 differentially contribute to functional networks: Fp1 was involved in cognition, working memory and perception, whereas Fp2 was part of brain networks underlying affective processing and social cognition. The present study thus disclosed cortical correlates of a functional segregation of the human frontopolar cortex. The

*Corresponding author. s.bludau@fz-juelich.de (S. Bludau).

Conflict of interest

The authors declare that there is no conflict of interest.

probabilistic maps provide a sound anatomical basis for interpreting neuroimaging data in the living human brain, and open new perspectives for analyzing structure–function relationships in the prefrontal cortex. The new data will also serve as a starting point for further comparative studies between human and non-human primate brains. This allows finding similarities and differences in the organizational principles of the frontal lobe during evolution as neurobiological basis for our behavior and cognitive abilities.

Introduction

Brodmann area (BA) 10 is located at the frontal pole of the human brain and represents the most rostral part of the brain. It is part of the prefrontal cortex (PFC). Its large extent in the human brain as compared to other species (Semendeferi et al., 2001) makes it a candidate for processing “human-specific” functions. BA10 is involved in many higher cognitive functions such as planning of future actions and the ability to draw analogies (Fuster, 2008). There are several theories (reviewed by e.g. Ramnani and Owen (2004) or Tsujimoto et al. (2011)), like the gateway hypotheses (Burgess et al., 2005, 2007) or the hypotheses of cognitive branching (Koechlin et al., 1999) which try to combine the variety of neuroimaging findings.

The precise localization of the borders of BA10 using structural or functional MRI is not possible. In contrast to the primary sensory areas with their distinct cyto- and myeloarchitecture (Zilles and Amunts, 2010, 2012), the relatively similar architecture of the various six-layered isocortical areas of the prefrontal cortex does not provide sufficient tissue contrast for *in vivo* mapping of such subtle differences. *In vivo* mapping approaches, which predict the localization of areal borders by cortical folding patterns work well in primary cortical areas, but are less successful in higher associative areas (Fischl et al., 2008, 2009; Hinds et al., 2008, 2009). Using high-field MRI and the myelin-based contrast allowed delineating the primary visual cortex (Geyer et al., 2011), but a definition of borders of higher associative cortical areas and higher sensory areas like that on the human frontal pole could not be demonstrated until now. Such MR-derived myelin maps are impaired in regions close to air/tissue interfaces, like the orbitofrontal cortex and the frontal pole adjacent to the frontal sinus (Glasser and Van Essen, 2011) because of susceptibility artifacts. Delineating cortical regions based on connectivity patterns taken from diffusion weighted MRI in living subjects is another *in vivo* option which might lead to localization of higher order cortical areas, but this approach requires reliably and precisely defined regions of interest for fiber tracking (Behrens and Johansen-Berg, 2005; Johansen-Berg et al., 2004). In the vast majority of areas, the delineation of cytoarchitectonic areas of the isocortex provides presently the only precise, reliable and reproducible basis for anatomical localization of functional studies and independent evaluation of structural *in vivo* mapping approaches.

The cytoarchitectonic map of Korbinian Brodmann (Brodmann, 1909) (Fig. 1A) shows an area BA10, occupying the frontal pole including the frontomarginal sulcus, the rostral part of the superior frontal gyrus and small parts of the middle frontal gyrus. Caudally, BA10 is bordered by middle frontal area BA46. The mesial border to BA32 is located rostral to the

cingulate gyrus. The rostral end of the olfactory sulcus could be taken as a gross macroscopic landmark for the borderline to orbitofrontal area BA11 according to Brodmann's map. A comparable cytoarchitectonic map (Fig. 1B) was proposed by (von Economo and Koskinas (1925) and Sarkisov and the Russian school (Fig. 1C) (Sarkisov et al., 1949).

In a more recently published map (Öngür et al., 2003), area 10 is subdivided into three parts, 10 m, 10r, and 10p (Fig. 1D). Area 10p occupies the frontal pole, while 10 m and 10r are found on the lower part of the mesial surface of the frontal lobe. The map of Öngür and colleagues differs from the older maps by the larger extent of area 10 on the mesial surface of the brain. It shows 10 m and 10r as a broad "tongue" extending on the most ventral part of the cingulate gyrus.

Thus, the parcellations of area 10 provided by these maps differ regarding the number of subdivisions as well as the extent of the areas. This might reflect interindividual anatomical variability of the extent, and different parcellations methods and concepts in case of the number of subdivisions. The interindividual variability is an important aspect of cytoarchitectonic parcellations as shown by the probability maps of different cortical regions, e.g. various visual areas (Amunts et al., 2000; Malikovic et al., 2007), primary motor cortex (Geyer et al., 1996), primary and secondary somatosensory cortices (Eickhoff et al., 2006a, 2006b; Geyer et al., 1999, 2000; Grefkes et al., 2001), Broca's region (Amunts et al., 1999), primary auditory cortex (Morosan et al., 2001), and parietal cortex (Caspers et al., 2006; Eickhoff et al., 2006a). These factors influencing cortical parcellation schemes have been discussed elsewhere (Zilles and Amunts, 2010).

Furthermore, existing maps of the frontal pole have not been published in a format, which enables comparisons with functional imaging data in a common spatial reference system. This is important, because recent functional studies showed different activations for the lateral and medial part of the frontal pole (Burgess et al., 2003; Gilbert et al., 2007, 2010; Schilbach et al., 2010).

The aim of the present study was to investigate if the functional differentiation into a medial and lateral region within area 10 is reflected by cytoarchitecture, and to generate three-dimensional, probabilistic maps. The borders of cytoarchitectonic areas were delineated in serial histological sections of 10 postmortem brains using an observer-independent approach (Schleicher et al., 1999, 2000, 2005, 2009). Two new areas, Fp1 and Fp2, were found by quantitative cytoarchitectonic criteria, and probability maps were generated in a standard reference space, which capture the intersubject variability in localization and extent, and provide a common reference system for comparison with functional imaging data. In order to better understand the functional role of the two identified areas, these new cytoarchitectonic maps served as regions of interest for a consecutive coordinate-based meta-analysis.

Material and methods

Histological processing of postmortem brains

Ten brains, 5 females and 5 males, were obtained via the body donor program of the Department of Anatomy at the University of Düsseldorf, Germany (Table 1). Postmortem delay of brain extraction ranged between 8 and 13 h. Clinical records did not show neurological or psychiatric diseases. Written informed consent was obtained according to the body donor program by the University of Düsseldorf governed by the local ethics committee. Histological processing has been performed as previously described (Amunts et al., 1999). In short, each brain was fixed in formalin or in Bodian's fixative for at least 6 months. The complete brains were embedded in paraffin and serially sectioned on a microtome (Polycut E, Reichert-Jung, Germany; thickness = 20 μm). Approximately 5500 to 8000 sections, depending on the individual brain size, were obtained. The sample used in the present study included three brains cut in the coronal plane and seven brains cut horizontally. Every 15th section was mounted onto a gelatine-covered glass slide, corresponding to 300 μm distance between mounted sections, and stained for cell bodies using a modified silver method (Merker, 1983).

Observer-independent detection of cytoarchitectonic borders based on the analysis of the grey level index (GLI)

The delineation of areas was based on an observer-independent mapping approach (Amunts and Zilles, 2001; Schleicher et al., 1999, 2005, 2009; Zilles et al., 2002). To this end, rectangular regions of interest (ROIs) were defined in the histological sections and digitized with a CCD-Camera (Axiocam MRm, ZEISS, Germany), which was connected to an optical light microscope (Axioplan 2 imaging, ZEISS, Germany). The camera and the motor-operated stage of the microscope were controlled by the Zeiss image analysis software KS400 (version 3.0) and Axiovision (version 4.6).

ROIs were digitized with an in-plane resolution of 1.02 μm per pixel (Fig. 2A). Gray-level index (GLI) (Schleicher and Zilles, 1990) images were calculated with KS400 and in-house software written in MatLab (The MathWorks, Inc., Natick, MA). Each pixel in a GLI image represents a measure of the volume fraction of cell bodies (Wree et al., 1982) in a measuring field of 16×16 pixel in the original digitized ROI (Figs. 2E,F), and therefore reflect aspects of cytoarchitectonic organization of the ROI. In the next step, an outer (between layers I and II) and inner contour line (between layer VI and the white matter) (Fig. 3A) were defined. Between both contour lines, curvilinear traverses were calculated using a physical model based on electric field lines (Jones et al., 2000) (Fig. 3A). Extracting the GLI values along those traverses led to profiles which could be operationalized with ten features (Dixon et al., 1988; Schleicher et al., 2009; Zilles et al., 2002): mean GLI value, centre of gravity in x-direction, standard deviation, skewness, kurtosis, and analogous parameters of the profiles' first derivatives. Each profile was re-sampled with linear interpolation to a standard length corresponding to a cortical thickness of 100% (0% = border between layers I and II; 100% = border with white matter), so that profiles of different lengths could be compared. The extracted features were combined in a ten-element feature vector, which was used to calculate the Mahalanobis distance (MD; Mahalanobis et al., 1949) between two adjacent

regions of profiles as a measure for dissimilarity between profiles (Mahalanobis et al., 1949; Schleicher et al., 2000) (Fig. 3E).

For observer-independent border detection, a specified number of profiles (block size from 10 to 24 profiles) were combined into a block of profiles. The calculation of the Mahalanobis distance was performed using a sliding window procedure for each profile position and all block sizes surrounding this position (range: 10–24 profiles) across the whole cortical ribbon as enclosed by the contour lines (Schleicher et al., 1999, 2000, 2005; Schleicher and Zilles, 1990). So the MD between two adjacent regions could be used as an observer independent measurement for cytoarchitectonic differences.

Significant maxima of the distance function for different block sizes were found at those positions of profiles where the mid-point of the sliding window was located over a cytoarchitectonic border between two adjacent cortical areas using a Hotelling's T2 statistic with Bonferroni correction (Schleicher et al., 1999).

3D reconstruction and probabilistic maps

The extent of the delineated areas Fp1 and Fp2 was interactively transferred to high-resolution scans (1200 dpi; ~20 $\mu\text{m}/\text{pixel}$; 8 bit grey value resolution) of the respective histological sections. All histological data sets and the mapped area 10 were 3D-reconstructed. The 3D-reconstruction was based on (i) the structural magnetic resonance image (MRI) 3D data set of the fixed brain obtained before sectioning and (ii) high-resolution flatbed scans of the stained histological sections (Amunts et al., 1999). The comparison of these datasets allowed correcting for deformations and shrinkage inevitably caused by histological techniques, (Amunts et al., 2004; Henn et al., 1997; Mohlberg et al., 2003). To generate a stereotaxic map and to account for inter-individual anatomical variability, the extent of the delineated areas of all examined brains was spatially normalized and transferred to the T1-weighted single-subject template of the Montreal Neurological Institute (MNI) brain (Evans et al., 1992). Linear and nonlinear elastic registration tools were applied (Henn et al., 1997; Hömke, 2006). The delineated cytoarchitectonic areas were superimposed in this reference brain template, and probabilistic maps were calculated. The probability that a cortical area was found at a certain position, in each voxel in the reference brain, was characterized by values from 0% to 100%, and color-coded.

Subsequently, a maximum probability map (MPM) was calculated (Eickhoff et al., 2005, 2006b). Hereby, each voxel was assigned to the cytoarchitectonic area with the highest probability in this voxel (Eickhoff et al., 2005). To correctly allocate those voxels which showed equal probabilities, the neighboring voxels were used to aid in classification. A threshold of 40% was applied at those border regions of Fp1 and Fp2, where the two delineated areas bordered regions which have not been mapped with the observer independent algorithm used for the present analysis (e.g., BA46 at the dorsolateral border, and BA9 at the dorsal border of area Fp1 (Eickhoff et al., 2005; Scheperjans et al., 2008). Finally, we calculated the surface of the maximum probability map by computing the area associated with each vertex of the midplane surface and subsequently summed up all area values which were labeled with Fp1 resp. Fp2. The associated area of a vertex is given by one third of the sum of the areas of the adjacent triangles. Due to the fact that the surface

was calculated based on the maximum probability map in the reference space of the T1-weighted single-subject template of the Montreal Neurological Institute (MNI) brain (Evans et al., 1992) we had to correct these values by a factor of 1.439. This factor was calculated by comparing the volumes of the (smaller) individual postmortem brains against the volume of the reference brain.

Volumetric analysis of areas Fp1 and Fp2

Fresh total volumes of each analyzed brain were estimated from its fresh weight and a mean density of 1.033 g/mm³ (Kretschmann and Wingert, 1971). To compensate for shrinkage due to histological processing, an individual correction factor was defined for each postmortem brain as the ratio between its fresh volume and its histological volume (Amunts et al., 2007). The fresh volumes of the delineated areas were stereologically estimated in each hemisphere using the high-resolution flatbed scan delineations and Cavalieri's principle (Gundersen et al., 1988).

The volume of areas Fp1 and Fp2 in each brain was also expressed as a fraction of total brain volume (area volume proportion: volume area/brain volume, [%]) in order to make the results comparable for brains differing in their absolute weight. Differences of the volume proportion of areas Fp1 and Fp2 were tested for significant effects of hemisphere and gender differences with pair-wise permutation tests using in-house software written in MatLab (Eickhoff et al., 2007). For each of these tests, the corresponding values (male/female; left/right hemisphere) were grouped and a contrast estimate was calculated between the means of these groups. The null distribution was estimated by Monte-Carlo simulation (Table 3). All values were randomly redistributed into two groups, calculating the same contrast with a repetition of 1,000,000 iterations. The difference between the two areas was considered significant if the contrast estimate of the true comparison was larger than 95% of the values under random (i.e., null) distribution ($P < 0.05$; Eickhoff et al., 2007) (Table 3). Correlations between volume and age were analyzed by building the Spearman correlation coefficient.

Meta-analytic connectivity modelling

A coordinate based meta-analysis was performed using a revised activation likelihood estimation (ALE) technique (Eickhoff et al., 2009, 2012; Laird et al., 2005; Turkeltaub et al., 2002) based on the BrainMap database. This approach determines the convergence of (co-activation) foci reported from different experiments that activate the delineated regions. The foci were modeled as probability distributions based on the spatial uncertainty due to the between-subject and between-template variability of neuroimaging data. Therefore, a location query was performed within the BrainMap database (www.brainmap.org, (Fox and Lancaster, 2002)) for studies activating Fp1 and Fp2. The MPM including the cytoarchitectonically defined areas from this study was used to define regions of interest. From that database, only those experiments were considered, that reported stereotaxic coordinates from normal mapping studies (no interventions and no group comparison) in healthy subjects using either fMRI or PET. These inclusion criteria yielded (at the time of analysis) approximately 5000 functional neuroimaging experiments. Note that we considered all eligible BrainMap experiments because any preselection of taxonomic categories would constitute a fairly strong a priori hypothesis about how brain networks are

organized. The main idea of the ALE algorithm is to treat the reported foci as centres for 3D Gaussian probability distributions to capture the spatial uncertainty associated with each focus. The algorithm shows statistical convergence of reported activations across different experiments found via the BrainMap search query. The results are interpreted under the assumption that the observed clusters have a higher probability than given only random convergence. To identify random and non-random foci clusters the obtained ALE values were compared with a null-distribution reflecting a random spatial association between the considered experiments (Eickhoff et al., 2012). The analysis was thresholded at a cluster-level FWE corrected $p < 0.05$ (cluster-forming threshold at voxel-level $p < 0.001$).

Results

Cytoarchitecture of the human frontal pole

General characteristics—Areas Fp1 and Fp2 represent typical isocortical areas with six layers. The border between layers II and III was clear cut (Fig. 4). Layer II consisted of a high amount of granular cells, which were intermingled by pyramidal cells of very small size from layer III. Consequently, the impression of a well demarcated border to layer III was mainly caused by the much lower cell density in upper layer III as compared to layer II. Layer III showed a gradient in pyramidal cell size from superficial (larger cells) to deep parts (smaller cells), reaching a medium size of the pyramids in lower layer III. One of the most characteristic criteria for the identification of the frontopolar areas was the structure of layer IV: it was broad and showed a high cell density (Fig. 4). The borders to layers III and V were well defined. The upper part of layer V showed high cell density and small- to medium-sized pyramidal cells. In contrast to that, lower parts of V showed lower cell density and medium-sized pyramidal cells. Layer VI was thick, and showed high cell density in its upper part. The transition with the white matter was blurred, mainly because of the low cell density in its lower portion (Fig. 4).

Two cytoarchitecturally distinct areas, Fp1 (lateral) and Fp2 (medial) were identified based on quantitative criteria and a multivariate distance measure according to an observer independent border detection approach (Schleicher et al., 1999, 2000, 2005 Schleicher and Zilles, 1990). The border between them was approximately located at the margin of the interhemispheric fissure. Area Fp1 occupied rostral parts of the superior and middle frontal gyri, whereas area Fp2 was located at the rostral mesial superior frontal gyrus. Area Fp1 showed higher cell density in layer II and in lower parts of layer III, and a broader layer IV than area Fp2 (Figs. 4A,B). Upper Layer V in area Fp2 mainly consisted of medium sized pyramid cells which caused the impression of a small belt next to layer IV (Fig. 4C). Relatively sharp borders between layers I, II and III, and a well-developed layer IV were characteristic for both areas and distinguished them from neighboring areas.

Cytoarchitectonic borders of areas Fp1 and Fp2 with neighboring cortical areas and corresponding gross macroscopic landmarks

Areas Fp1 and Fp2 are surrounded by areas 9, 11, 32 and 46 according to Brodmann's map (1909; Fig. 1A). The identification of cytoarchitectonic areas 9 and 46 was based on studies of Rajkowska and Goldman-Rakic (Rajkowska and Goldman-Rakic, 1995a, b). Criteria for

the medially located neighbor BA32 were taken from publications by Palomero-Gallager and Vogt (Palomero-Gallagher et al., 2008; Vogt et al., 1995). A summary of the cytoarchitectonic features could be found in Table 2.

Cytoarchitectonic border with BA9

BA9 was located caudo-dorsally to area Fp1, mainly on the superior, and also partially on the mesial frontal gyrus. In BA9, layer III contained medium sized pyramidal cells throughout the entire layer. As in area Fp1, layer II and layer IV were clearly visible, but layer IV (and to a lesser degree layer II) showed a less sharp border with their neighboring layers than area Fp1 (Fig. 5). The structure of layer IV was one of the most important criteria for distinguishing BA9 from area Fp1: layer IV in BA9 showed a lower cell density, and was not as broad as layer IV of area Fp1 (Fig. 5B). In Fig. 5B, layer IV is located at 43% to 51% cortical width as compared to 42% to 55% for layer IV of area Fp1. One reason for the sharp border with layer V in area Fp1 was the high cell density of upper layer V (Figs. 5A,B), which was not that prominent in BA9. The superimposed mean profile of area Fp1 quantified the high cell density of upper layer V, with a distinct peak from reaching from 53% to 63% cortical width (Fig. 5B), which was much smaller than the corresponding peak in the mean profile of BA9 from 52% to 63% cortical width. A significant maximal Mahalanobis distance was found at profile position 55, and indicated the border between both areas (Fig. 5C). The described differences in cytoarchitecture led to observer-independent detectable borders of the frontopolar regions with BA9, which were located on the rostral end of the superior frontal gyrus.

Cytoarchitectonic border with BA11

BA11 was mostly located on the gyrus rectus, ventrally to areas Fp1 and Fp2. The cortical ribbon of BA11 was very thin (Fig. 6). The considerable difference in widths of the cortex of area Fp2 and BA11 was accompanied by a more blurred transition of layer VI to the white matter in area Fp2 as compared to BA11. Another difference between the cytoarchitecture of area Fp1 and Fp2 on the one hand, and BA11 on the other was found with respect to layer III. Layer III of Fp1 and Fp2 showed a gradient in pyramidal cell size from superficial to deep parts (Fig. 6), whereas in BA11 such a gradient in the size of the pyramidal cells was not as prominent. Layer IV, one of the most prominent cytoarchitectonic characteristics of the frontopolar areas, was thinner in BA11 than in areas Fp1 and Fp2, and showed a less sharp border with layer III as a result of the irregular alignment of pyramidal cells in layer III (Fig. 6). Both cytoarchitectonic areas showed high cell density in the upper part of layer V.

The border between the Fp-areas and BA11 was mainly located at the medial/dorsal end of the gyrus rectus and the rostral end of the olfactory sulcus.

Cytoarchitectonic border of area Fp1 with BA46

BA46 was the dorsal neighbor of area Fp1 on the middle frontal gyrus. Layer II in area 46 showed a high cell density with a less precise border with layer III, compared to the layer II/III border of neighboring area Fp1 (Fig. 7). Layer IV was clearly visible, despite being less prominent with lower cell density than in area Fp1. One of the most consistent

cytoarchitectonic characteristics to differ between area Fp1 and BA46 was the composition of the infragranular layers V and VI. In contrast to area Fp1, BA46 showed a more homogenous layer V and the intersection between layer VI and the white matter in BA46 was sharper caused by the more homogenous infragranular layers of BA46. The border of area Fp1 with BA46 was not associated with any macroscopical landmark.

Cytoarchitectonic border with BA32

BA32 was the mesial, dorsal neighbor of area Fp2. The most prominent difference between both areas was found with respect to layer IV. BA32, in contrast to area Fp2, was a dysgranular area, i.e. layer IV in BA32 was not well developed as an independent, consistent layer, and only few granular cells were found, which intermingled with pyramidal cells from layers III and V (Fig. 8). In addition, BA32 showed a relatively broad layer II with high cell density (Fig. 8). Layer III showed medium-sized pyramidal cells throughout the entire layer, and few larger pyramidal cells in lower layer III. Some of these larger pyramidal cells reached into layer IV, thus providing a less sharp border between the layers as compared to area Fp2. Viewing BA32 with a low magnification revealed layers Va and VI as clearly visible dark curves separated by a lighter curve caused by the low cell density of layer Vb.

The paracingulate sulcus served as a gross macroscopic landmark for the border of area Fp2 with BA32.

Volumetric analysis of areas Fp1 and Fp2

The average total volume V (\pm SD) of areas Fp1 and Fp2 ($n = 20$ hemispheres) of one hemisphere was $6390 \text{ mm}^3 \pm 1351 \text{ mm}^3$ (left hemispheres: $7235 \text{ mm}^3 \pm 1165 \text{ mm}^3$; right hemispheres: $6610 \text{ mm}^3 \pm 1566 \text{ mm}^3$ /female: $5858 \text{ mm}^3 \pm 1193 \text{ mm}^3$; male: $6922 \text{ mm}^3 \pm 1342 \text{ mm}^3$) (Table 3, Fig. 9). The combined volume of areas Fp1 and Fp2 of one hemisphere in each brain was also expressed as a proportion of total brain volume (left hemispheres: $0.51\% \pm 0.07$; right hemispheres: $0.47\% \pm 0.09$ /female: $0.47\% \pm 0.09$; male: $0.50\% \pm 0.08$) (Table 3). The interhemispheric differences of the volume proportion of the frontal areas Fp1 and Fp2 compared to the entire brain volume showed strong variations, with a largest range from 0.31% to 0.49% between two hemispheres (Table 3). Nevertheless, the permutation test showed no significant differences of the volume proportions between hemispheres or genders and no significant interaction between both. The correlation test showed no interaction between volume and age ($r = -0.55$, $p = 0.097$).

Probabilistic and maximum probability map (MPM) of areas Fp1 and Fp2

In order to quantify the inter-individual variability in the extent and location of areas Fp1 and Fp2, both areas were registered onto the MNI reference brain (Figs. 10, 11). The superimposition of all ten brains showed that the frontal pole is completely covered by areas Fp1 and Fp2. Due to the interindividual anatomical variability of the areas, voxels in the periphery of the maps with low overlap (i.e., probabilities; blue) were more frequent than central voxels/vertices with high overlap (red) (Fig. 11). Therefore, the maps of areas Fp1 and Fp2 overlapped at lower frequencies. A non-overlapping parcellation of the frontal pole was obtained by combining the individual probabilistic maps and creating that area Fp1 occupied the polar part including the frontomarginal sulcus, the rostral part of the superior

frontal gyrus and small parts of the middle frontal gyrus. Area Fp2 was located at the rostral mesial part of the superior frontal gyrus. The mesial/dorsal end of the gyrus rectus and the rostral end of the olfactory sulcus could be taken as gross macroscopic landmarks for the border between area Fp2 and BA11. The MPM illustrates that the border between area 10 and BA32 is approximately defined by the anterior end of the cingulate gyrus (Figs. 12B,C). The ensuing surface areas [mm²] are: left Fp2 = 807.33, left Fp1 = 3258.66, right Fp2 = 1050.63, and right Fp1 = 3041.50. In order to verify the calculated surface areas we compared it to our volume data. Assuming a mean cortical thickness of 2.5 mm for the polar part of the human brain according to von Economo and Koskinas (1925) and multiplying it with our calculated surface areas led to a volume of 10,164 mm³ for left area 10 and 10,230 mm³ for right area 10. The corrected volumes are 7063 mm³ for the left, and 7109 mm³ for the right area 10, which is well comparable with the volumes of the present study (left hemispheres: 7235 mm³ ± 1165 mm³; right hemispheres: 6610 mm³ ± 1566 mm³). The cytoarchitectonic maps are shown as surface projections onto the MNI brain at http://www.fz-juelich.de/inm/inm-1/jubrain_cytoviewer.

Coordinate based meta-analysis of functional imaging studies reporting area Fp1 and area Fp2 activations

In order to approach the function of the two new areas, a coordinatebased meta-analysis of areas Fp1 and Fp2 co-activations within functional imaging studies was performed. Both areas showed several significant co-activation clusters (Fig. 13). The largest co-activation clusters for areas Fp1 and Fp2 were located on the posterior and middle cingulated cortex of both hemispheres (Fig. 13, Table 4). Parts of the left angular gyrus (left inferior parietal cortex (PGa, (Caspers et al., 2008)) also co-activated with both delineated areas. In addition to that, areas Fp1 and Fp2 showed co-activation patterns which were unique for the specific area. Only Fp1 showed co-activations in left area 44 (Amunts et al., 1999), right inferior parietal lobule (PFm, (Caspers et al., 2008)), right mid-orbitofrontal gyrus and left area 6 (Geyer, 2004). In contrast, left putamen, left area 2 (Grefkes et al., 2001), left middle temporal gyrus and the right laterobasal group of the amygdala (Amunts et al., 2005) showed co-activations with area Fp2. Coordinates of the activation maxima of the meta-analysis are given in Table 4. Thus, areas Fp1 and Fp2 differed not only cytoarchitectonically, but also with respect to co-activation patterns and their behavioral domains as assigned according to the BrainMap classification (www.brainmap.org, (Fox and Lancaster, 2002)). Fp1 was involved in cognition, working memory and perception, whereas Fp2 was part of brain networks underlying affective processing and social cognition (Fig. 14).

Discussion

The present study entailed a three-dimensional, cytoarchitectonic map of the human frontal pole, which considers its interindividual variability. It is based on observer-independently detected borders and is available in the MNI reference space, where it can be directly compared to results of functional imaging studies. BA10 has been subdivided into two cytoarchitectonically distinct areas: area Fp1 located laterally and Fp2 located medially. The

cytoarchitectonic-based map was used for a coordinate-based meta-analysis of functional imaging studies reporting activations within areas Fp1 and Fp2.

Comparison of the new frontal pole map with architectonic maps

The localization and extent of areas Fp1 and Fp2 taken together agrees with the cytoarchitectonic work of Brodmann. The dorsal, medial border of area Fp2 with BA32 is located rostrally to the cingulate gyrus, which is comparable to Brodmann's delineation of BA10. In contrast to Brodmann's map, the present study provided evidence of a subdivision into a medial and a lateral area based on an observer-independent cytoarchitectonic approach. The map of Von Economo and Koskinas (1925) defined in addition to the Area frontopolaris several transitional regions surrounding this area. Transitional areas encompass areas "Fem" and "Femd" dorsally, area "Fef" laterally, and area "Fel" medially. Including all those transitional regions into the extent of BA10 would lead to an overestimation of the extension of area 10 as identified in the present study. Those transitional regions thus likely reflect parts of areas surrounding area 10. The transitional area defined on the medial wall (Fel) also exceeded the gross macroscopic landmark for the medial border of area Fp2, and encompasses the cingulate gyrus, which is occupied by area 32, and not by any transitional area as shown in similar postmortem brains (Brodmann, 1909; Palomero-Gallagher et al., 2008; Vogt et al., 1995). The border between areas "Fe" and "Fel" described by von Economo and Koskinas (1925) matched well with the border of Fp2 and area 32.

The present study differs in some aspects from a recent cytoarchitectonic map of the orbital and medial prefrontal cortex (Öngür et al., 2003). The latter subdivided the medial part of area 10 into an anterior area 10r and a more posterior area 10 m, whereby the areas at the mesial surface showed a larger extent in caudal direction (Fig. 1D) than those delineated in the present study. The posterior subregion 10 m covered a major part of the paracingulate sulcus, which is located on the medial wall of the brain (Palomero-Gallagher et al., 2008; Vogt et al., 1995). The extent of subarea 10 m is in contrast to a more recent map published by Vogt and Palomero-Gallagher (Palomero-Gallagher et al., 2008; Vogt et al., 1995). It is also in contrast to the results of the present study, which identified Fp2 on the medial wall with the cingulate sulcus as gross macroscopic landmark for its border to area 32. In contrast to Öngür and colleagues, the observer-independent approach for defining cytoarchitectonic borders did not support the notion of a further subdivision of area Fp2. On the other hand, the cytoarchitectonic criteria for area Fp2 are compatible with those of area 10r of Öngür et al. (2003).

Comparison of volumetric and cytoarchitectonic analyses of areas Fp1 and Fp2 with recent human and great ape studies

The human frontal pole with areas Fp1 and Fp2 is one of the largest brain regions in the human brain. For example, the mean volume of area Fp1 is up to two times larger than the largest areas of the inferior parietal lobule (Caspers et al., 2008). The same holds true for a comparison with human areas 44 and 45 of Broca's region (Amunts et al., 1999), and with areas 5 Ci, 5 M, and 5 L of the superior parietal cortex (Scheperjans et al., 2008). Larger volumes have been reported for primary areas BA17 (23.2 cm³; SD 3.6) and BA18 (19.5 cm³; SD 3.7) (Amunts et al., 2000). The permutation test of the analyzed volumetric datasets

showed no significant differences in volume for factors hemisphere and gender as well as no significant interaction between them. This is plausible since the main functions associated with the anterior prefrontal cortex are higher cognitive functions, which deal with bilateral input of other association areas (Gilbert et al., 2010).

The volume of area Fp1 and Fp2 is not only larger than that of any other higher association area in the human brain, but also larger than homologous areas in non-human primates (chimpanzee 2239 mm³, bonobo 2804 mm³, orang-utan 1611 mm³, gibbon 203 mm³ as shown by Semendeferi (1994) and Semendeferi et al. (2001)). Semendeferi et al. (2001) reported a volume of 14,217 mm³ for the right area 10, which is more than two times higher than our mean volume of 6610 ± 1566 mm³ for the right areas Fp1 + Fp2. This discrepancy is probably caused by an overestimation of the extent of area 10 in this study. Their area 10 occupied parts of the orbitofrontal cortex as indicated in an earlier publication (see Fig. 5.1 in Semendeferi (1994)), which was the basis for the publication in 2001. This orbitofrontal region was clearly part of the orbitofrontal cortex as shown in several more recent maps by Hof et al. (1995), Öngür et al. (2003), Mackey and Petrides (2009) and Uylings et al. (2010). Moreover, the mapping in 1994 was not based on an observer-independent method for defining the borders, which was introduced only later (Schleicher et al., 1999). I.e., the volume estimates of the 2001 publication considerably overestimated the size of area 10. Nonetheless the criteria used to delineate area 10 in the 2001 publication were consistently used across the primate species studied and the human brain, so the validity of the comparative aspects of that study is not questioned here.

Homologies between non-human primate areas and corresponding human brain areas were defined according to a comparable topology and cytoarchitecture as described by Semendeferi et al. (Semendeferi et al., 2001, 2011). However, human BA10 differs from that of the great apes by a lower cell density, corresponding to a higher neuropil fraction, and thus by more space for connections in human brains as compared to other primates (Semendeferi et al., 2011; Spocter et al., 2012). In fact, a higher number of dendritic spines per cell, and considerably more connections to the supramodal cortex has been shown (Jacobs et al., 1997, 2001). In combination with the differences in volume, this recent finding was interpreted as supragranular layers of BA10 in humans would have more space for connections with other higher-order association areas as compared to other primates. Based on the higher number of dendritic spines per cell, another theory emerged, stating that the anterior prefrontal cortex might have computational properties for the integration of incoming information, which are different from those of other brain areas (Ramnani and Owen, 2004). These characteristics suggest that the human rostral PFC, as a phylogenetically young area (Fuster, 2002, 2008), is likely to support processes of integration or coordination of inputs. This feature might have particularly developed in humans (Amodio and Frith, 2006; Burgess et al., 2005, 2007).

Co-activations of areas Fp1 and Fp2

Meta-analytic connectivity modeling seeded in cytoarchitecturally defined areas Fp1 and Fp2 revealed significant differences in the co-activation patterns of these two areas. Our results thus corroborate previous results (Gilbert et al., 2010) indicating different task-based

functional connectivity patterns for the medial and a lateral part of the frontal pole. In contrast to the database-driven and hence unbiased approach of the present study, however, the study by Gilbert et al. (2010) was based on a database of different functional imaging studies, which showed activations in rostral prefrontal cortex. The current findings rely on a large and diverse set of studies stored in the BrainMap database that were filtered by the presence of activation foci in the cytoarchitecturally defined areas. Importantly, reference to such a large dataset also allowed quantitative behavioral characterization by testing for behavioral domains or paradigm classes that were significantly overrepresented among the experiments activating Fp1 and Fp2, respectively. Hence we could show differences in functional co-activation and associated behavioral domains between two histologically defined regions in a quantitative, observer-independent approach.

Recent studies showed a functional segregation of the lateral and medial part of the frontal pole (Burgess et al., 2003; Gilbert et al., 2007,2010; Schilbach et al., 2010). A differential activation of the medial and lateral aspect of area 10 was demonstrated for the suppression and maintenance of internally-generated thoughts (Burgess et al., 2003), and behavioral measures (lateral activations were associated with tasks with slow response times and vice versa;(Gilbert et al., 2006a)). There are also hints for a possible split into three functional subregions of the human frontal pole based on different activations to cognitive and emotional tasks (Gilbert et al., 2006b) and analogical reasoning (Volle et al., 2010). In these studies, a medial posterior region was described which corresponds well with Fp2 described in the present study. However, we could not find a division of Fp1 into two subregions based on our cytoarchitectonic observations. In summary, the available data suggest a subdivision of the frontopolar region, not mentioned in the maps of Brodmann (1909), von Economo and Koskinas (1925), and Sarkisov et al. (1949).

The human frontal pole has been associated with many higher mental functions, in particular planning and social behavior. First hints towards these may be found in the classical description of Phineas Gage (Harlow, 1848, 1863). Further lesion studies analysing the anterior frontal cortex followed, leading to several theories about planning deficits (Burgess et al., 2001; Dreher et al., 2008; Grafman, 1995; Shallice, 1982). While these studies indicated the importance of the frontopolar cortex for managing multiple, time shifted goals, the present study indicates that presumably “abstract cognitive” and “social cognitive” processing (and presumably planning, may be differentially processed within this region.

Our study showed that area Fp1 is functionally connected with inferior frontal as well as parietal regions and, together with these, preferentially activated by episodic and working memory tasks. Episodic memory as a specific aspect of long-term memory is related to specific events in one’s past as opposed to general (semantic) knowledge. In contrast, working memory refers to the time-limited active storage of information for further operation such as recombination, comprehension and comparison (e.g. in the ‘n-back’ tasks (Nyberg et al., 2003; Owen et al., 2005)). Both episodic and working memory form key foundations of other higher cognitive functions such as planning and organization of future actions, i.e., typical functions associated with the frontal pole (Goel and Grafman, 2000). Based on our findings, we would propose, that these more “abstract cognitive” aspects of the frontal pole should primarily be implemented by area Fp1. In turn, this region may thus be

considered an important substrate for organized behavior, planning of actions and managing multiple goals based on both episodic and short-term memory information.

Contrasting this “abstract cognitive” role of area FP1, area Fp2 was mainly involved in emotional as well as social cognition tasks and functionally connected to the lateral temporal lobe, the right laterobasal group of the amygdala and the right hippocampus. The laterobasal group of the amygdala is the largest part of a complex of subnuclei of the human amygdala (Amunts et al., 2005). Different studies showed that a major amount of subcortical and cortical inputs converge to the laterobasal group (McDonald, 1998; Phelps and LeDoux, 2005) and it seems to be important to assign emotional value to the converged sensory stimuli (Sah et al., 2003). All of the latter regions have likewise been implicated in affective, inter-personal (Mitchell et al., 2002, 2005) and higher-order social cognitive functions (Fletcher et al., 1995; Goel et al., 1995; Johnson et al., 2002; Kelley et al., 2002). We may thus conclude that affective and social-cognitive abilities, including the planning of future behavior in an inter-personal context and the adequate maintainable of social roles would mainly be implemented in the medial aspect of the frontal pole. In summary, looking back at the classical description of Phineas Gage and the wealth of subsequent literature on patients with frontal pole damage pointing to difficulties in organizing cognitive planning and social behavior, we would argue, that these two deficits should have discernible neural substrates. Whereas abstract planning and memory functions are mainly attributable to Fp1 and its network, affective and social processing is mainly subserved by Fp2 and its connections.

Outlook

The present study demonstrated significant regional differences in the cytoarchitecture of the human frontopolar cortex. The probability maps of two new areas, Fp1 and Fp2, are steps toward a complete map of the human prefrontal cortex based on observer-independent criteria. The coordinate-based, meta-analysis showed different co-activation patterns for the delineated areas within the human frontal pole. This underlined that a detailed and observer-independently delineated map of the areas may contribute to the understanding of the correlation of the microstructural segregation of the frontal cortex and its functional segregation.

The data on the cytoarchitectonic parcellation of the frontal pole can now be used as anatomical constraints for a more detailed in-vivo mapping approach, which might be beneficial for the interpretation of functional neuroimaging and diffusion-weighted MRI studies (Behrens and Johansen-Berg, 2005; Blaizot et al., 2010; Johansen-Berg et al., 2004). The referred studies demonstrate a combination of cytoarchitectonic maps and datasets obtained via functional or diffusion-weighted MRI as they used the cytoarchitectonically precisely defined regions as seed regions for their subsequent analysis. The combination with connectivity-based parcellation, meta-analytic connectivity modeling, and in-vivo mapping approaches will reveal the structural, connectional, and functional properties of the human frontal pole in the future.

Acknowledgments

This study was supported by the BMBF (01GW0612, K.A.). Further funding was granted by the Helmholtz Alliance for Mental Health in an Aging Society (HelMA; K.A., K.Z.) and by the Helmholtz Alliance on Systems Biology (Human Brain Model; K.Z., S.B.E.). The authors thank Katerina Semendeferi for critical review of the manuscript and for helpful discussions.

References

- Amodio DM, Frith CD. Meeting of minds: the medial frontal cortex and social cognition. *Nat. Rev. Neurosci.* 2006; 7:268–277. [PubMed: 16552413]
- Amunts K, Zilles K. Advances in cytoarchitectonic mapping of the human cerebral cortex. *Neuroimaging Clin. N. Am.* 2001; 11:151–169. [PubMed: 11489732]
- Amunts K, Schleicher A, Burgel U, Mohlberg H, Uylings HB, Zilles K. Broca's region revisited: cytoarchitecture and intersubject variability. *J. Comp. Neurol.* 1999; 412:319–341. [PubMed: 10441759]
- Amunts K, Malikovic A, Mohlberg H, Schormann T, Zilles K. Brodmann's areas 17 and 18 brought into stereotaxic space—where and how variable? *NeuroImage.* 2000; 11:66–84. [PubMed: 10686118]
- Amunts K, Weiss PH, Mohlberg H, Pieperhoff P, Eickhoff S, Gurd JM, Marshall JC, Shah NJ, Fink GR, Zilles K. Analysis of neural mechanisms underlying verbal fluency in cytoarchitectonically defined stereotaxic space—the roles of Brodmann areas 44 and 45. *NeuroImage.* 2004; 22:42–56. [PubMed: 15109996]
- Amunts K, Kedo O, Kindler M, Pieperhoff P, Mohlberg H, Shah NJ, Habel U, Schneider F, Zilles K. Cytoarchitectonic mapping of the human amygdala, hippocampal region and entorhinal cortex: intersubject variability and probability maps. *Anat. Embryol. (Berl.)*. 2005; 210:343–352. [PubMed: 16208455]
- Amunts K, Armstrong E, Malikovic A, Homke L, Mohlberg H, Schleicher A, Zilles K. Gender-specific left-right asymmetries in human visual cortex. *J. Neurosci.* 2007; 27:1356–1364. [PubMed: 17287510]
- Behrens TE, Johansen-Berg H. Relating connective architecture to grey matter function using diffusion imaging. *Philos. Trans. R. Soc. Lond. B Biol. Sci.* 2005; 360:903–911. [PubMed: 16087435]
- Blaizot X, Mansilla F, Insausti AM, Constans JM, Salinas-Alaman A, Pro-Sistiaga P, Mohedano-Moriano A, Insausti R. The human parahippocampal region: I. Temporal pole cytoarchitectonic and MRI correlation. *Cereb. Cortex.* 2010; 20:2198–2212. [PubMed: 20064939]
- Brodmann, K. Vergleichende Lokalisationslehre der Großhirnrinde in ihren Prinzipien dargestellt auf Grund des Zellenbaues. Leipzig: Verlag von Johann Ambrosius Barth; 1909.
- Burgess PW, Quayle A, Frith CD. Brain regions involved in prospective memory as determined by positron emission tomography. *Neuropsychologia.* 2001; 39:545–555. [PubMed: 11257280]
- Burgess PW, Scott SK, Frith CD. The role of the rostral frontal cortex (area 10) in prospective memory: a lateral versus medial dissociation. *Neuropsychologia.* 2003; 41:906–918. [PubMed: 12667527]
- Burgess, PW., Simons, JS., Dumontheil, I., Gilbert, SJ. The gateway hypothesis of rostral prefrontal cortex (area 10) function. In: Duncan, J., Phillips, L., McLeod, P., editors. *Measuring the Mind: Speed, Control, and Age.* Oxford: Oxford University Press; 2005. p. 217–248.
- Burgess PW, Dumontheil I, Gilbert SJ. The gateway hypothesis of rostral prefrontal cortex (area 10) function. *Trends Cogn. Sci.* 2007; 11:290–298. [PubMed: 17548231]
- Caspers S, Geyer S, Schleicher A, Mohlberg H, Amunts K, Zilles K. The human inferior parietal cortex: cytoarchitectonic parcellation and interindividual variability. *NeuroImage.* 2006; 33:430–448. [PubMed: 16949304]
- Caspers S, Eickhoff SB, Geyer S, Scheperjans F, Mohlberg H, Zilles K, Amunts K. The human inferior parietal lobule in stereotaxic space. *Brain Struct. Funct.* 2008; 212:481–495.
- Dixon, W., Brown, M., Engelman, L., Hill, M., Jennrich. *BMDP statistical software.* Berkeley University of California Press; 1988.

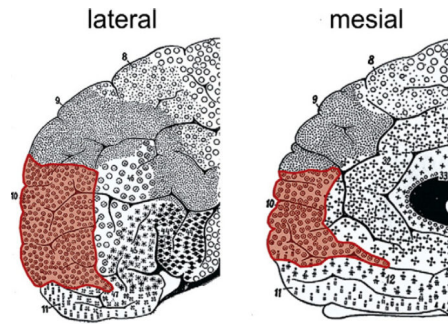
- Dreher JC, Koechlin E, Tierney M, Grafman J. Damage to the fronto-polar cortex is associated with impaired multitasking. *PLoS One*. 2008; 3:e3227. [PubMed: 18795100]
- Eickhoff SB, Stephan KE, Mohlberg H, Grefkes C, Fink GR, Amunts K, Zilles K. A new SPM toolbox for combining probabilistic cytoarchitectonic maps and functional imaging data. *NeuroImage*. 2005; 25:1325–1335. [PubMed: 15850749]
- Eickhoff SB, Amunts K, Mohlberg H, Zilles K. The human parietal operculum. II. Stereotaxic maps and correlation with functional imaging results. *Cereb. Cortex*. 2006a; 16:268–279. [PubMed: 15888606]
- Eickhoff SB, Heim S, Zilles K, Amunts K. Testing anatomically specified hypotheses in functional imaging using cytoarchitectonic maps. *NeuroImage*. 2006b; 32:570–582. [PubMed: 16781166]
- Eickhoff SB, Schleicher A, Scheperjans F, Palomero-Gallagher N, Zilles K. Analysis of neurotransmitter receptor distribution patterns in the cerebral cortex. *NeuroImage*. 2007; 34:1317–1330. [PubMed: 17182260]
- Eickhoff SB, Laird AR, Grefkes C, Wang LE, Zilles K, Fox PT. Coordinate-based activation likelihood estimation meta-analysis of neuroimaging data: a random-effects approach based on empirical estimates of spatial uncertainty. *Hum. Brain Mapp*. 2009; 30:2907–2926. [PubMed: 19172646]
- Eickhoff SB, Bzdok D, Laird AR, Kurth F, Fox PT. Activation likelihood estimation meta-analysis revisited. *NeuroImage*. 2012; 59:2349–2361. [PubMed: 21963913]
- Evans AC, Marrett S, Neelin P, Collins L, Worsley K, Dai W, Milot S, Meyer E, Bub D. Anatomical mapping of functional activation in stereotactic coordinate space. *NeuroImage*. 1992; 1:43–53. [PubMed: 9343556]
- Fischl B, Rajendran N, Busa E, Augustinack J, Hinds O, Yeo BT, Mohlberg H, Amunts K, Zilles K. Cortical folding patterns and predicting cytoarchitecture. *Cereb. Cortex*. 2008; 18:1973–1980. [PubMed: 18079129]
- Fischl B, Stevens AA, Rajendran N, Yeo BT, Greve DN, Van Leemput K, Polimeni JR, Kakunoori S, Buckner RL, Pacheco J, Salat DH, Melcher J, Frosch MP, Hyman BT, Grant PE, Rosen BR, van der Kouwe AJ, Wiggins GC, Wald LL, Augustinack JC. Predicting the location of entorhinal cortex from MRI. *NeuroImage*. 2009; 47:8–17. [PubMed: 19376238]
- Fletcher PC, Happe F, Frith U, Baker SC, Dolan RJ, Frackowiak RS, Frith CD. Other minds in the brain: a functional imaging study of “theory of mind” in story comprehension. *Cognition*. 1995; 57:109–128. [PubMed: 8556839]
- Fox PT, Lancaster JL. Opinion: mapping context and content: the BrainMap model. *Nat Rev. Neurosci*. 2002; 3:319–321. [PubMed: 11967563]
- Fuster JM. Frontal lobe and cognitive development. *J. Neurocytol*. 2002; 31:373–385. [PubMed: 12815254]
- Fuster, JiM. *The Prefrontal Cortex*. London, London: Acad. Press; 2008.
- Geyer S. The microstructural border between the motor and the cognitive domain in the human cerebral cortex. *Adv. Anat Embryol. Cell Biol*. 2004; 174:1–89.
- Geyer S, Ledberg A, Schleicher A, Kinomura S, Schormann T, Burgel U, Klingberg T, Larsson J, Zilles K, Roland PE. Two different areas within the primary motor cortex of man. *Nature*. 1996; 382:805–807. [PubMed: 8752272]
- Geyer S, Schleicher A, Zilles K. Areas 3a, 3b, and 1 of human primary somatosensory cortex. *NeuroImage*. 1999; 10:63–83. [PubMed: 10385582]
- Geyer S, Schormann T, Mohlberg H, Zilles K. Areas 3a, 3b, and 1 of human primary somatosensory cortex. Part 2. Spatial normalization to standard anatomical space. *NeuroImage*. 2000; 11:684–696. [PubMed: 10860796]
- Geyer S, Weiss M, Reimann K, Lohmann G, Turner R. Microstructural parcellation of the human cerebral cortex—from Brodmann’s post-mortem map to in vivo mapping with high-field magnetic resonance imaging. *Front Hum Neurosci*. 2011; 5:19. [PubMed: 21373360]
- Gilbert SJ, Spengler S, Simons JS, Frith CD, Burgess PW. Differential functions of lateral and medial rostral prefrontal cortex (area 10) revealed by brain-behavior associations. *Cereb. Cortex*. 2006a; 16:1783–1789. [PubMed: 16421331]

- Gilbert SJ, Spengler S, Simons JS, Steele JD, Lawrie SM, Frith CD, Burgess PW. Functional specialization within rostral prefrontal cortex (area 10): a meta-analysis. *J. Cogn. Neurosci.* 2006b; 18:932–948. [PubMed: 16839301]
- Gilbert SJ, Williamson ID, Dumontheil I, Simons JS, Frith CD, Burgess PW. Distinct regions of medial rostral prefrontal cortex supporting social and nonsocial functions. *Soc. Cogn. Affect. Neurosci.* 2007; 2:217–226. [PubMed: 18985143]
- Gilbert SJ, Gonen-Yaacovi G, Benoit RG, Volle E, Burgess PW. Distinct functional connectivity associated with lateral versus medial rostral prefrontal cortex: a meta-analysis. *NeuroImage.* 2010; 53:1359–1367. [PubMed: 20654722]
- Glasser MF, Van Essen DC. Mapping human cortical areas in vivo based on myelin content as revealed by T1- and T2-weighted MRI. *J. Neurosci.* 2011; 31:11597–11616. [PubMed: 21832190]
- Goel V, Grafman J. Role of the right prefrontal cortex in ill-structured planning. *Cogn. Neuropsychol.* 2000; 17:415–436. [PubMed: 20945189]
- Goel V, Grafman J, Sadato N, Hallett M. Modeling other minds. *Neuroreport.* 1995; 6:1741–1746. [PubMed: 8541472]
- Grafman J. Similarities and distinctions among current models of prefrontal cortical functions. *Ann. N. Y. Acad. Sci.* 1995; 769:337–368. [PubMed: 8595036]
- Grefkes C, Geyer S, Schormann T, Roland P, Zilles K. Human somatosensory area 2: observer-independent cytoarchitectonic mapping, interindividual variability, and population map. *NeuroImage.* 2001; 14:617–631. [PubMed: 11506535]
- Gundersen HJ, Bendtsen TF, Korbo L, Marcussen N, Moller A, Nielsen K, Nyengaard JR, Pakkenberg B, Sorensen FB, Vesterby A, et al. Some new, simple and efficient stereological methods and their use in pathological research and diagnosis. *APMIS.* 1988; 96:379–394. [PubMed: 3288247]
- Harlow JM. Passage of an iron rod through the head. *Boston Med. Surg. J.* 1848; 39:389–393.
- Harlow JM. Recovery after severe injury to the head. *Publications of the Massachusetts Medical Society.* 1863; 2:327–346.
- Henn, S., Schormann, T., Engler, K., Zilles, K., Witsch, K. Elastische Anpassung in der digitalen Bildverarbeitung auf mehreren Auflösungsstufen mit Hilfe von Mehrgitterverfahren. In: Paulus, E., Wahl, FM., editors. *Mustererkennung.* Berlin: Springer; 1997. p. 392-399.
- Hinds OP, Rajendran N, Polimeni JR, Augustinack JC, Wiggins G, Wald LL, Diana Rosas H, Potthast A, Schwartz EL, Fischl B. Accurate prediction of V1 location from cortical folds in a surface coordinate system. *NeuroImage.* 2008; 39:1585–1599. [PubMed: 18055222]
- Hinds O, Polimeni JR, Rajendran N, Balasubramanian M, Amunts K, Zilles K, Schwartz EL, Fischl B, Triantafyllou C. Locating the functional and anatomical boundaries of human primary visual cortex. *NeuroImage.* 2009; 46:915–922. [PubMed: 19328238]
- Hof PR, Mufson EJ, Morrison JH. Human orbitofrontal cortex: cytoarchitecture and quantitative immunohistochemical parcellation. *J. Comp. Neurol.* 1995; 359:48–68. [PubMed: 8557847]
- Hömke L. A multigrid method for anisotropic PDEs in elastic image registration. *Numer. Linear Algebra Appl.* 2006; 13:215–229.
- Jacobs B, Driscoll L, Schall M. Life-span dendritic and spine changes in areas 10 and 18 of human cortex: a quantitative Golgi study. *J. Comp. Neurol.* 1997; 386:661–680. [PubMed: 9378859]
- Jacobs B, Schall M, Prather M, Kapler E, Driscoll L, Baca S, Jacobs J, Ford K, Wainwright M, Trembl M. Regional dendritic and spine variation in human cerebral cortex: a quantitative golgi study. *Cereb. Cortex.* 2001; 11:558–571. [PubMed: 11375917]
- Johansen-Berg H, Behrens TE, Robson MD, Drobjnjak I, Rushworth MF, Brady JM, Smith SM, Higham DJ, Matthews PM. Changes in connectivity profiles define functionally distinct regions in human medial frontal cortex. *Proc. Natl. Acad. Sci. U.S.A.* 2004; 101:13335–13340. [PubMed: 15340158]
- Johnson SC, Baxter LC, Wilder LS, Pipe JG, Heiserman JE, Prigatano GP. Neural correlates of self-reflection. *Brain.* 2002; 125:1808–1814. [PubMed: 12135971]
- Jones SE, Buchbinder BR, Aharon I. Three-dimensional mapping of cortical thickness using Laplace's equation. *Hum. Brain Mapp.* 2000; 11:12–32. [PubMed: 10997850]
- Kelley WM, Macrae CN, Wyland CL, Caglar S, Inati S, Heatherton TF. Finding the self? An event-related fMRI study. *J. Cogn. Neurosci.* 2002; 14:785–794. [PubMed: 12167262]

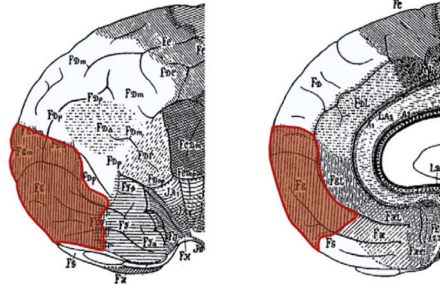
- Koechlin E, Basso G, Pietrini P, Panzer S, Grafman J. The role of the anterior prefrontal cortex in human cognition. *Nature*. 1999; 399:148–151. [PubMed: 10335843]
- Kovach CK, Daw ND, Rudrauf D, Tranel D, O’Doherty JP, Adolphs R. Anterior prefrontal cortex contributes to action selection through tracking of recent reward trends. *J. Neurosci*. 2012; 32:8434–8442. [PubMed: 22723683]
- Kretschmann, HJ., Wingert, F. *Computeranwendungen bei Wachstumsproblemen in Biologie und Medizin*. Berlin: Springer; 1971.
- Laird AR, Fox PM, Price CJ, Glahn DC, Uecker AM, Lancaster JL, Turkeltaub PE, Kochunov P, Fox PT. ALE meta-analysis: controlling the false discovery rate and performing statistical contrasts. *Hum. Brain Mapp*. 2005; 25:155–164. [PubMed: 15846811]
- Mackey S, Petrides M. Architectonic mapping of the medial region of the human orbitofrontal cortex by density profiles. *Neuroscience*. 2009; 159:1089–1107. [PubMed: 19356690]
- Mahalanobis P, Majumda D, Rao C. Anthropometric survey of the united provinces, 1941: a statistical study. *Sankhya*. 1949; 9:90–324.
- Malikovic A, Amunts K, Schleicher A, Mohlberg H, Eickhoff SB, Wilms M, Palomero-Gallagher N, Armstrong E, Zilles K. Cytoarchitectonic analysis of the human extrastriate cortex in the region of V5/MT+: a probabilistic, stereo-taxic map of area hOc5. *Cereb. Cortex*. 2007; 17:562–574. [PubMed: 16603710]
- McDonald AJ. Cortical pathways to the mammalian amygdala. *Prog. Neurobiol*. 1998; 55:257–332. [PubMed: 9643556]
- Merker B. Silver staining of cell bodies by means of physical development. *J. Neurosci. Methods*. 1983:235–241.
- Mitchell JP, Heatherton TF, Macrae CN. Distinct neural systems subserve person and object knowledge. *Proc. Natl. Acad. Sci. U.S.A.* 2002; 99:15238–15243. [PubMed: 12417766]
- Mitchell JP, Banaji MR, Macrae CN. General and specific contributions of the medial prefrontal cortex to knowledge about mental states. *NeuroImage*. 2005; 28:757–762. [PubMed: 16325141]
- Mohlberg, H., Lerch, J., Amunts, K., Evans, AC., Zilles, K. Probabilistic cytoarchitectonic maps transformed into MNI space. *Neuroimage (Proceedings of the Ninths International Conference on Functional Mapping of the Human Brain)*; 2003.
- Morosan P, Rademacher J, Schleicher A, Amunts K, Schormann T, Zilles K. Human primary auditory cortex: cytoarchitectonic subdivisions and mapping into a spatial reference system. *NeuroImage*. 2001; 13:684–701. [PubMed: 11305897]
- Nyberg L, Marklund P, Persson J, Cabeza R, Forkstam C, Petersson KM, Ingvar M. Common prefrontal activations during working memory, episodic memory, and semantic memory. *Neuropsychologia*. 2003; 41:371–377. [PubMed: 12457761]
- Öngür D, Ferry AT, Price JL. Architectonic subdivision of the human orbital and medial prefrontal cortex. *J. Comp. Neurol*. 2003; 460:425–449. [PubMed: 12692859]
- Owen AM, McMillan KM, Laird AR, Bullmore E. N-back working memory paradigm: a meta-analysis of normative functional neuroimaging studies. *Hum. Brain Mapp*. 2005; 25:46–59. [PubMed: 15846822]
- Palomero-Gallagher N, Mohlberg H, Zilles K, Vogt B. Cytology and receptor architecture of human anterior cingulate cortex. *J. Comp. Neurol*. 2008; 508:906–926. [PubMed: 18404667]
- Phelps EA, LeDoux JE. Contributions of the amygdala to emotion processing: from animal models to human behavior. *Neuron*. 2005; 48:175–187. [PubMed: 16242399]
- Rajkowska G, Goldman-Rakic PS. Cytoarchitectonic definition of prefrontal areas in the normal human cortex: I. Remapping of areas 9 and 46 using quantitative criteria. *Cereb. Cortex*. 1995a; 5:307–322. [PubMed: 7580124]
- Rajkowska G, Goldman-Rakic PS. Cytoarchitectonic definition of prefrontal areas in the normal human cortex: II. Variability in locations of areas 9 and 46 and relationship to the Talairach Coordinate System. *Cereb. Cortex*. 1995b; 5:323–337. [PubMed: 7580125]
- Ramnani N, Owen AM. Anterior prefrontal cortex: insights into function from anatomy and neuroimaging. *Nat. Rev. Neurosci*. 2004; 5:184–194. [PubMed: 14976518]
- Sah P, Faber ES, Lopez De Armentia M, Power J. The amygdaloid complex: anatomy and physiology. *Physiol. Rev*. 2003; 83:803–834. [PubMed: 12843409]

- Sarkisov, SA., Filimonoff, IN., Preobrashenskaya, NS. Cytoarchitecture of the human cortex cerebri (Russ.). Medgiz, Moscow: 1949.
- Scheperjans F, Eickhoff SB, Homke L, Mohlberg H, Hermann K, Amunts K, Zilles K. Probabilistic maps, morphometry, and variability of cytoarchitectonic areas in the human superior parietal cortex. *Cereb. Cortex.* 2008; 18:2141–2157. [PubMed: 18245042]
- Schilbach L, Wilms M, Eickhoff SB, Romanzetti S, Tepest R, Bente G, Shah NJ, Fink GR, Vogeley K. Minds made for sharing: initiating joint attention recruits reward-related neurocircuitry. *J. Cogn. Neurosci.* 2010; 22:2702–2715. [PubMed: 19929761]
- Schleicher A, Zilles K. A quantitative approach to cytoarchitectonics: analysis of structural inhomogeneities in nervous tissue using an image analyser. *J. Microsc.* 1990; 157:367–381. [PubMed: 2332886]
- Schleicher A, Amunts K, Geyer S, Morosan P, Zilles K. Observer-independent method for microstructural parcellation of cerebral cortex: a quantitative approach to cytoarchitectonics. *NeuroImage.* 1999; 9:165–177. [PubMed: 9918738]
- Schleicher A, Amunts K, Geyer S, Kowalski T, Schormann T, Palomero-Gallagher N, Zilles K. A stereological approach to human cortical architecture: identification and delineation of cortical areas. *J. Chem. Neuroanat.* 2000; 20:31–47. [PubMed: 11074342]
- Schleicher A, Palomero-Gallagher N, Morosan P, Eickhoff SB, Kowalski T, de Vos K, Amunts K, Zilles K. Quantitative architectural analysis: a new approach to cortical mapping. *Anat. Embryol. (Berl.).* 2005; 210:373–386. [PubMed: 16249867]
- Schleicher A, Morosan P, Amunts K, Zilles K. Quantitative architectural analysis: a new approach to cortical mapping. *J. Autism Dev. Disord.* 2009; 39:1568–1581. [PubMed: 19582566]
- Semendeferi, K. Evolution of the hominoid prefrontal cortex: a quantitative and image analysis of areas 13 and 10. Dissertation Graduate College, University of Iowa; 1994.
- Semendeferi K, Armstrong E, Schleicher A, Zilles K, Van Hoesen GW. Pre-frontal cortex in humans and apes: a comparative study of area 10. *Am. J. Phys. Anthropol.* 2001; 114:224–241. [PubMed: 11241188]
- Semendeferi K, Teffer K, Buxhoeveden DP, Park MS, Bludau S, Amunts K, Travis K, Buckwalter J. Spatial organization of neurons in the frontal pole sets humans apart from great apes. *Cereb. Cortex.* 2011; 21:1485–1497. [PubMed: 21098620]
- Shallice T. Specific impairments of planning. *Philos. Trans. R. Soc. Lond. B Biol. Sci.* 1982; 298:199–209. [PubMed: 6125971]
- Spocter MA, Hopkins WD, Barks SK, Bianchi S, Hehmeyer AE, Anderson SM, Stimpson CD, Fobbs AJ, Hof PR, Sherwood CC. Neupil distribution in the cerebral cortex differs between humans and chimpanzees. *J. Comp. Neurol.* 2012; 520:2917–2929. [PubMed: 22350926]
- Tsujimoto S, Genovesio A, Wise SP. Frontal pole cortex: encoding ends at the end of the endbrain. *Trends Cogn. Sci.* 2011; 15:169–176. [PubMed: 21388858]
- Turkeltaub PE, Eden GF, Jones KM, Zeffiro TA. Meta-analysis of the functional neuroanatomy of single-word reading: method and validation. *NeuroImage.* 2002; 16:765–780. [PubMed: 12169260]
- Uylings HB, Sanz-Arigita EJ, de Vos K, Pool CW, Evers P, Rajkowska G. 3-D cytoarchitectonic parcellation of human orbitofrontal cortex correlation with postmortem MRI. *Psychiatry Res.* 2010; 183:1–20. [PubMed: 20538437]
- Vogt BA, Nimchinsky EA, Vogt LJ, Hof PR. Human cingulate cortex: surface features, flat maps, and cytoarchitecture. *J. Comp. Neurol.* 1995; 359:490–506. [PubMed: 7499543]
- Volle E, Gilbert SJ, Benoit RG, Burgess PW. Specialization of the rostral pre-frontal cortex for distinct analogy processes. *Cereb. Cortex.* 2010; 20:2647–2659. [PubMed: 20156841]
- von Economo, C., Koskinas, GN. Die Cytoarchitektonik der Hirnrinde des erwachsenen Menschen. Berlin: Springer; 1925.
- Wree A, Schleicher A, Zilles K. Estimation of volume fractions in nervous tissue with an image analyzer. *J. Neurosci. Methods.* 1982; 6:29–43. [PubMed: 7121060]
- Zilles K, Amunts K. Centenary of Brodmann's map—conception and fate. *Nat. Rev. Neurosci.* 2010; 11:139–145. [PubMed: 20046193]

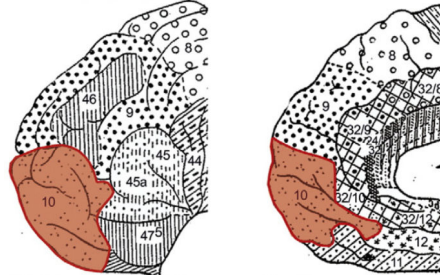
- Zilles, K., Amunts, K. Architecture of the human cerebral cortex: maps, regional and laminar organization. In: Paxinos, G., Mai, JK., editors. *The Human Nervous System*. Third. San Diego: Elsevier Academic Press; 2012. p. 836-895.
- Zilles, K., Schleicher, A., Palomero-Gallagher, N., Amunts, K. Quantitative analysis of cyto- and receptorarchitecture of the human brain. In: Toga, A., Mazziotta, J., editors. *Brain mapping: the methods*. 2nd. San Diego (CA): Academic Press; 2002. p. 573-602.



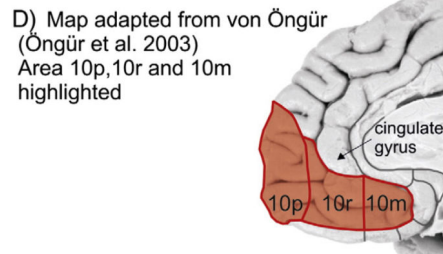
A) Map adapted from Brodmann (Brodmann 1909). BA 10 highlighted



B) Map adapted from von Economo & Koskinas (von Economo and Koskinas, 1925) Area F_c highlighted



C) Map adapted from von Sarkisov (Sarkisov et al., 1949). Area 10 highlighted



D) Map adapted from von Öngür (Öngür et al. 2003) Area 10p, 10r and 10m highlighted

Fig. 1.

Comparison of cytoarchitectonic maps of the human brain, frontal lobe. Differences between the former published cytoarchitectonic maps. Panels A, B, C illustrates the mesial part of area 10 as an extension below the cingulate gyrus which approximately ends caudally at the genu of the corpus callosum. Panel 1D: please note the large medial part of area 10, which is subdivided into 10 m and 10r. Area 10 m caudally extends below the genu of the corpus callosum.

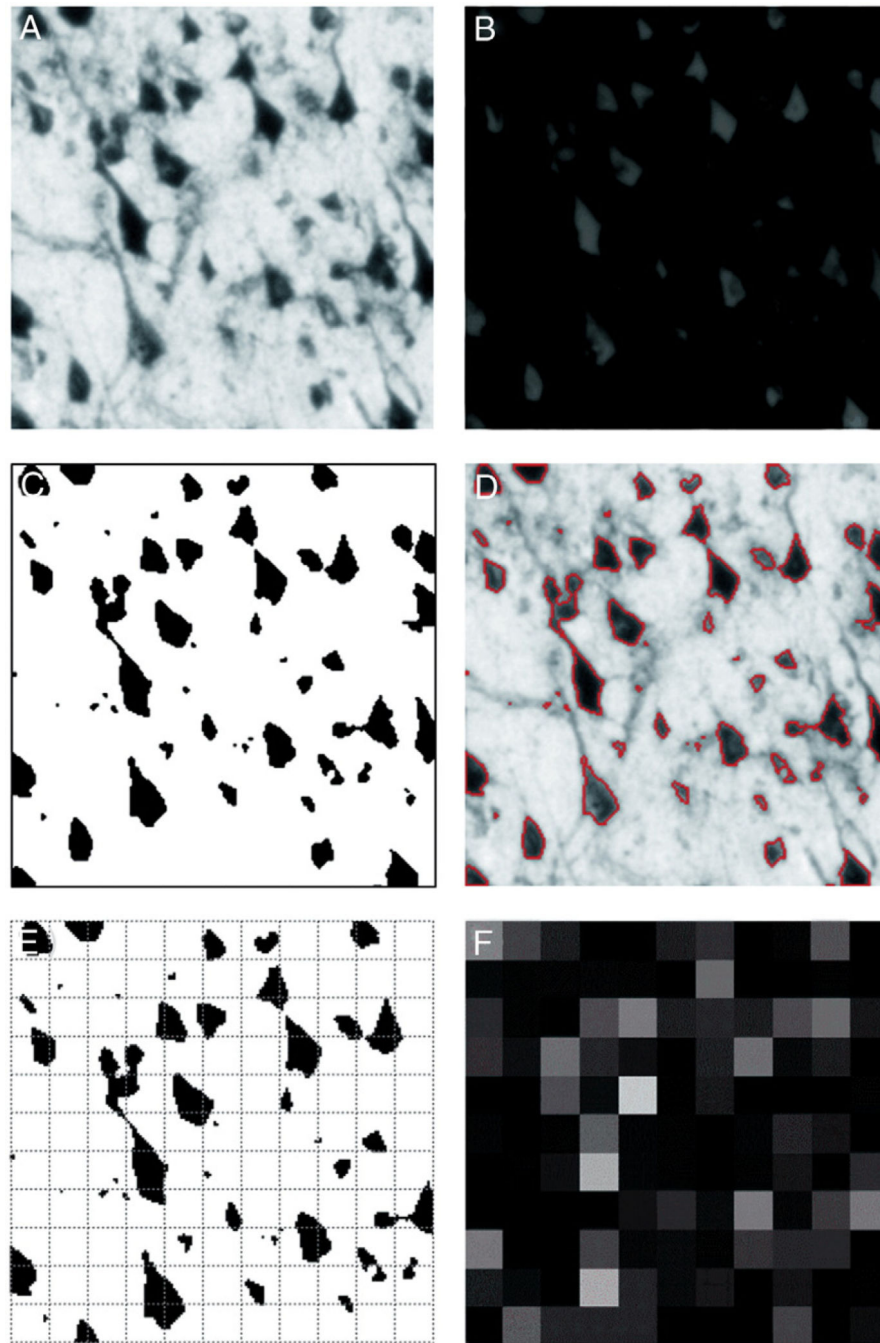


Fig. 2. Cell body detection using in-house software. Illustration of the different steps of image post-processing from the original digitized ROI A) to the cell body detection D). ROIs were digitized with an in-plane resolution of $1.02 \mu\text{m}$ per pixel A). Subsequent two Gauss filters, one with radius 1 pixel and one with radius 40 pixel were applied. For the edge detection of the cells the two resulting images were subtracted from each other B). ROIs were transferred to a binary image using a calculated threshold C). Image D) shows the binary overlay of the original image to visualise cell body detection. E) Binarized ROI

superimposed by a 16×16 grid which was used for the generation of GLI images. The corresponding GLI image rescaled to the same size (F). Each pixel in the GLI image represents an appraisalment for the volume fraction of cell bodies in a corresponding measuring field of size (16×16 pixel) in the original digitized ROI color coded by 8 bit grey values.

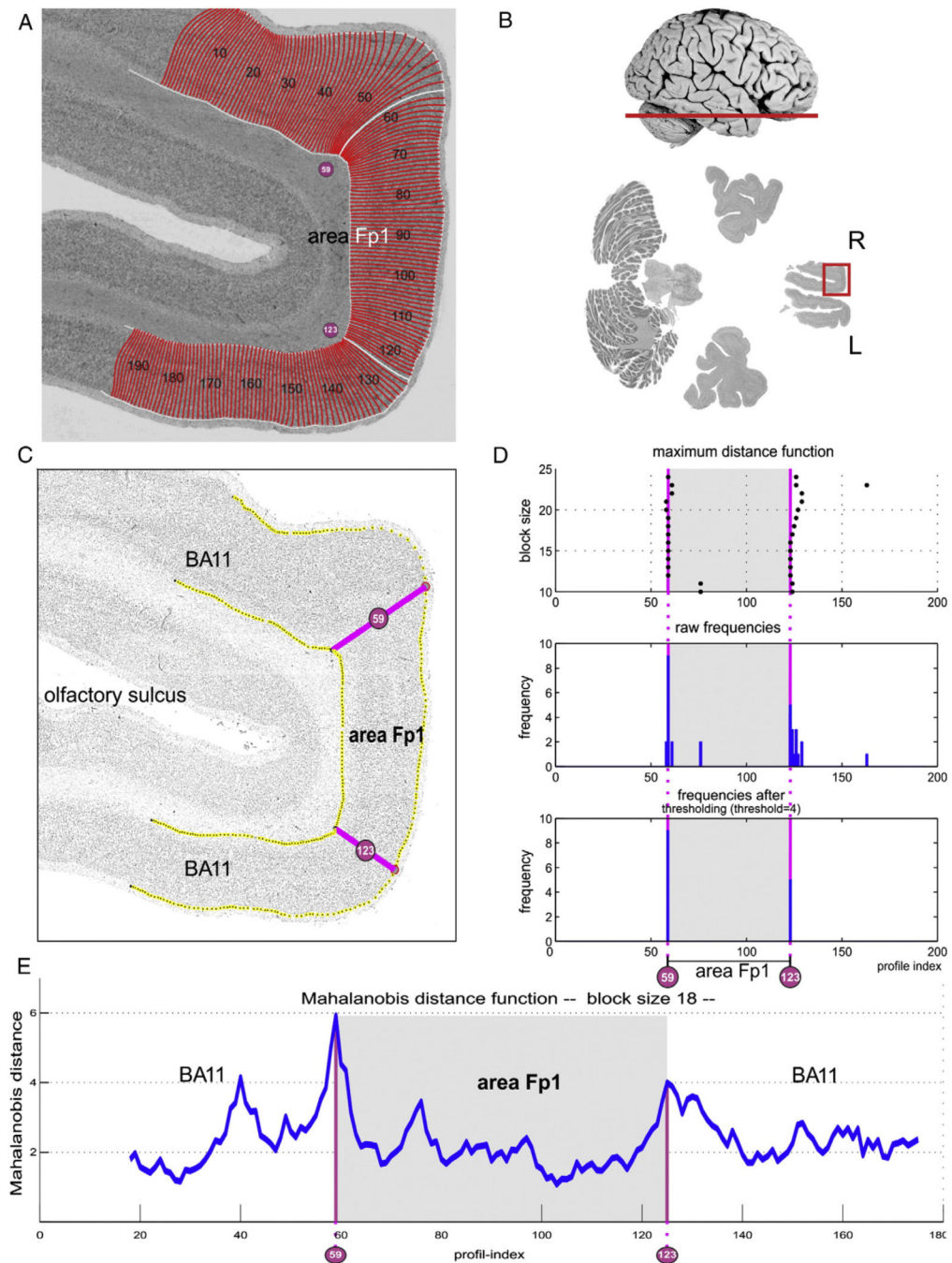


Fig. 3. Observer-independent border detection (Schleicher et al., 1999). A) Digitized ROI with contour lines and superimposed numbered curvilinear traverses (red lines) indicating where the GLI profiles were extracted. The bars at profile positions 59 and 123 corresponds to the significant maxima of the MD function in D–E caused by the cytoarchitectonic border between areas Fp1 and BA11 as confirmed by microscopical examination. (B) Horizontally cut cell-body stained brain section (thickness 20 μ m). The area in the red square corresponds to the analyzed ROI displayed in Figs. 3A–E. (D, “maximal distance function”) Dependence

of the position of significant maxima of the MD function (black dots) on the block size. Most dots are aligned at profile positions 59 and 123. (D, “raw frequencies”, “frequencies after thresholding”) Corresponding frequency of significant maxima at different profile positions across block sizes 10–24. The highest frequency occurred at profile positions 59 and 123, which were selected as putative cytoarchitectonic borders. (E) Single MD function at block size 18 with a significant maximum at profile positions 59 and 123.

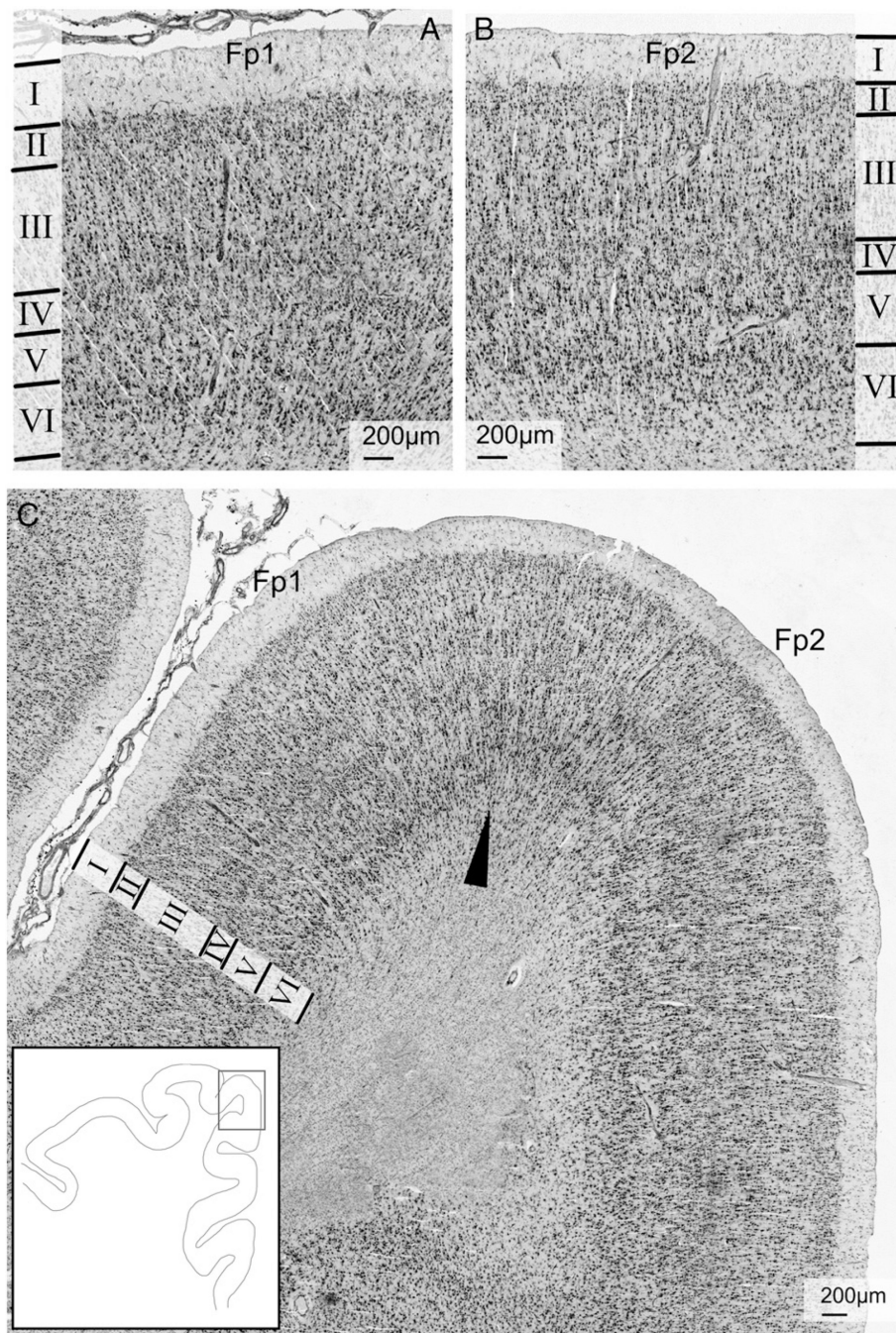


Fig. 4. Comparison of area Fp1 and Fp2 cytoarchitecture. A), B) Sharp border between layer I, layer II, layer III and layer IV with a high cell density was typical for area Fp1 and area Fp2. C) The lateral area Fp1 shows a broader layer II with a higher cell density, a higher cell density in lower parts of layer III, and a broader layer IV than the medial area Fp2. In addition to that, there was a small belt of pyramid cells in lower layer V of area Fp2, which could not be seen in area Fp1. Layers marked by roman numerals.

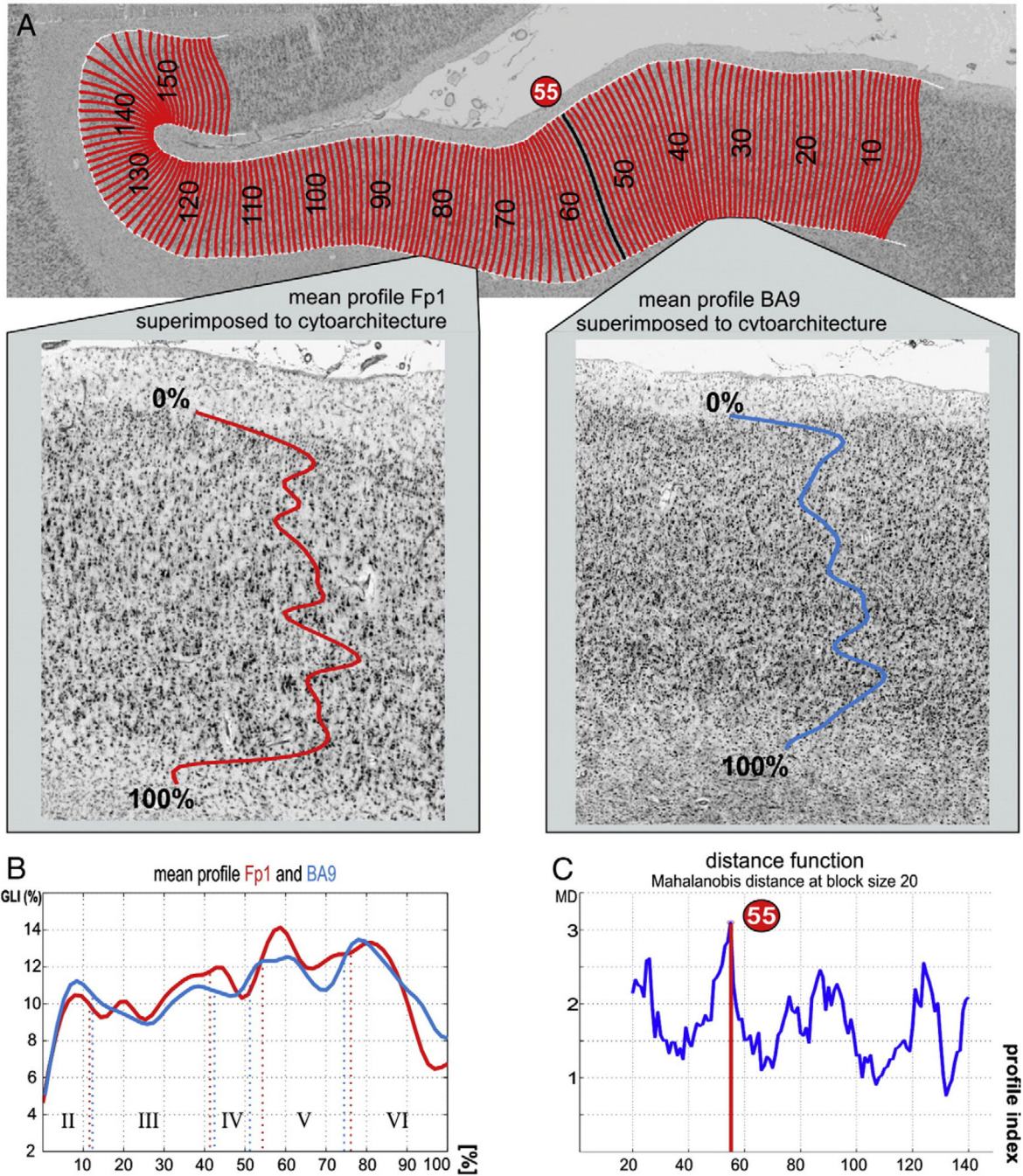


Fig. 5. Cytoarchitectonic differences between area Fp1 and BA9. A) Significant cytoarchitectonic border located at profile position 55. Grey boxes mark the position and width of the mean profiles, displayed within each grey box. B) Direct comparison of mean profile of Fp1 (red) and BA9 (blue). C) Exemplary Mahalanobis distance function and the distinct maximum at position 55, which leads to the observer-independent detected border.

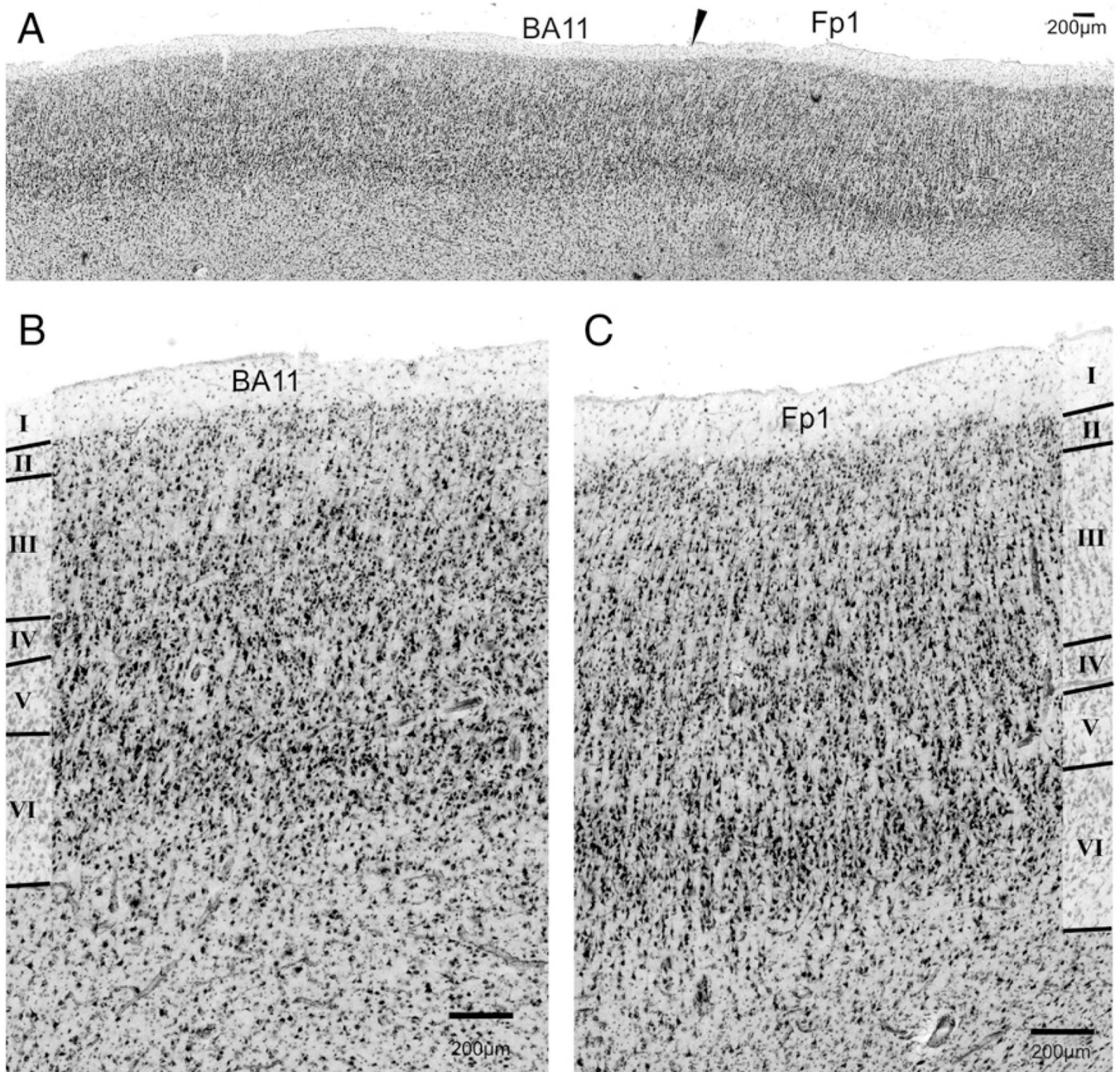


Fig. 6. Cytoarchitectonic border between area Fp1 and BA11 in microphotographs. Cytoarchitectonic border between area Fp1 and BA11 located on the Gyrus rectus A). BA11 and area Fp1 differed in cell density of layer IV (higher in Fp1 than in BA11) and with respect to cortex-white matter border (sharper in BA11 than in Fp1) (Figs. 6A,C).

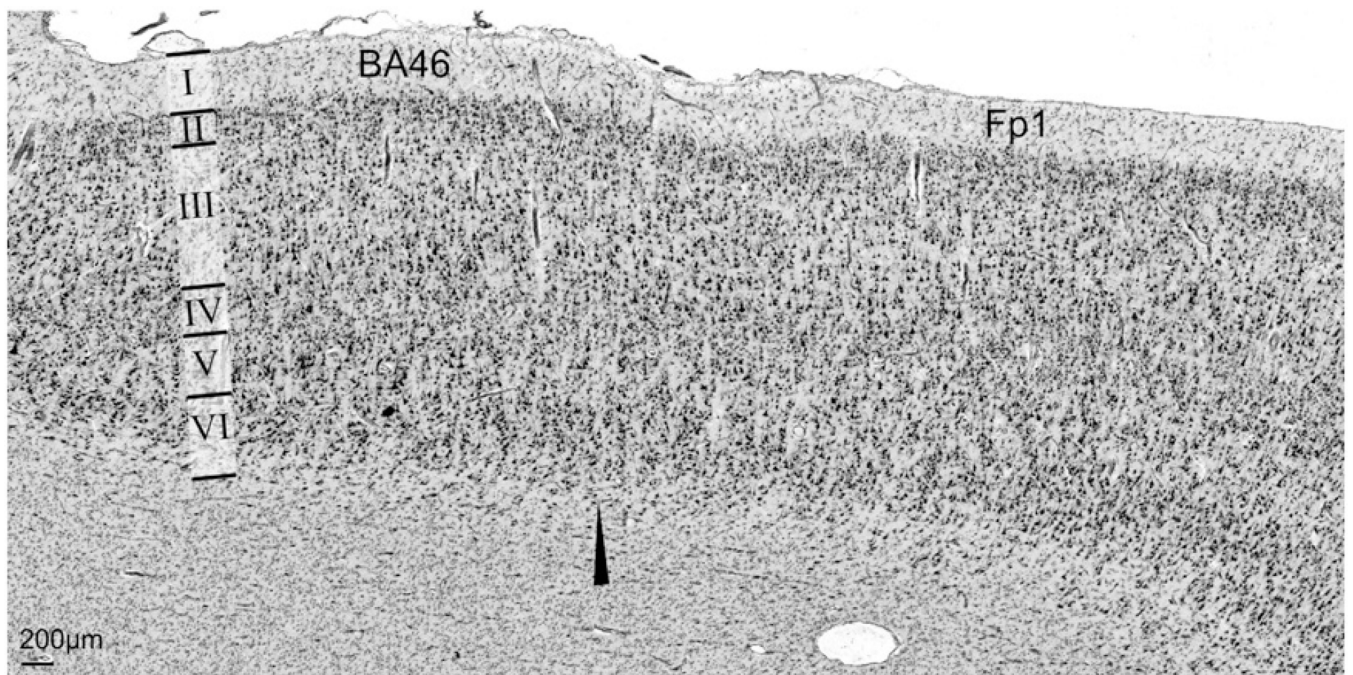


Fig. 7.

Cytoarchitectonic comparison of BA46 and area Fp1. Layer II in area Fp1 had a higher cell density and bordered sharper to layer III as layer II in BA46 does. The direct comparison showed the differences of the composition of the infragranular layers (more homogenous layer V in BA46, blurry intersection between layer VI and the white matter in area Fp1).

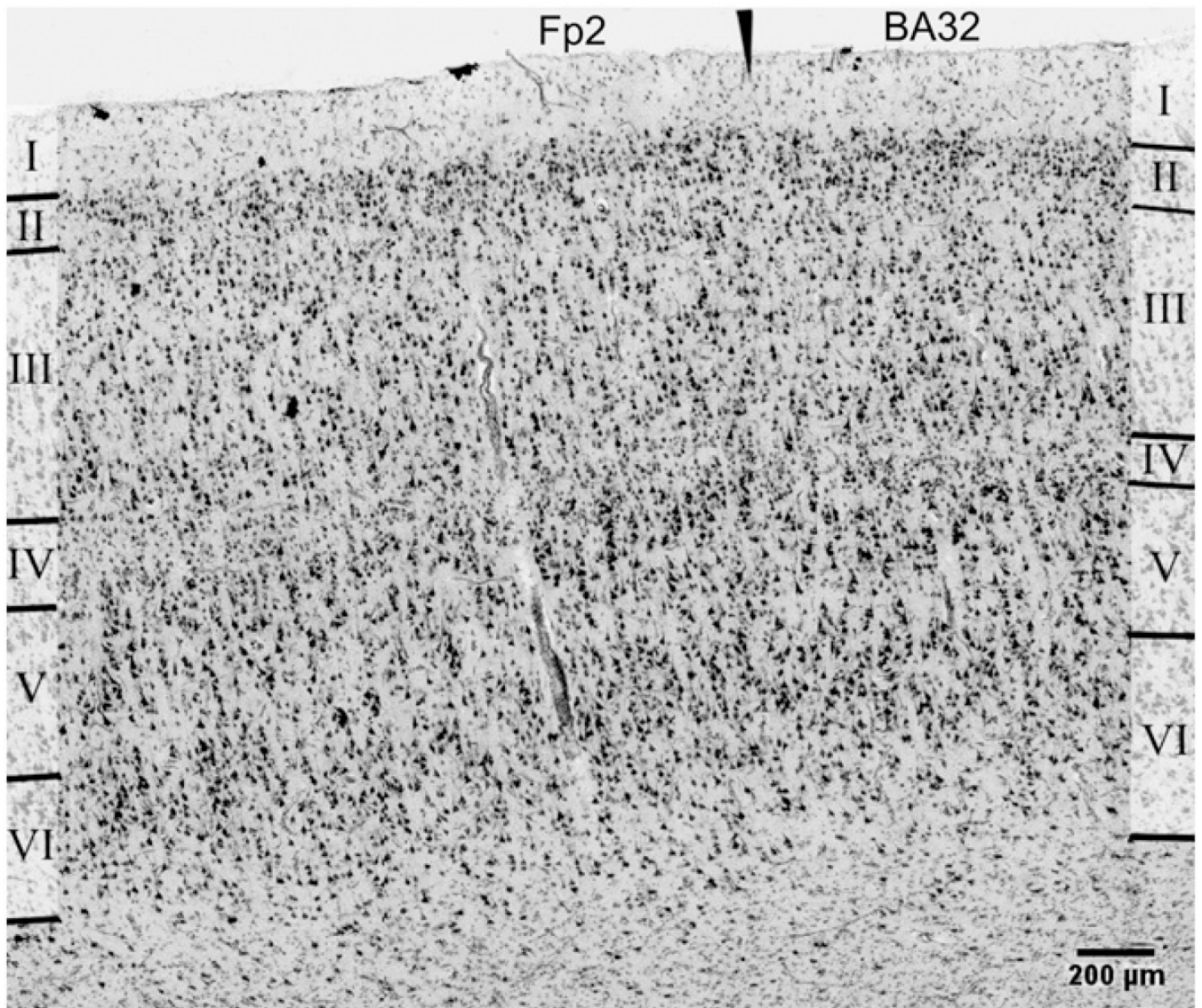


Fig. 8. Cytoarchitectonic border between area Fp2 and BA32. The arrow marks a border which was delineated using the observer independent border detection algorithm.

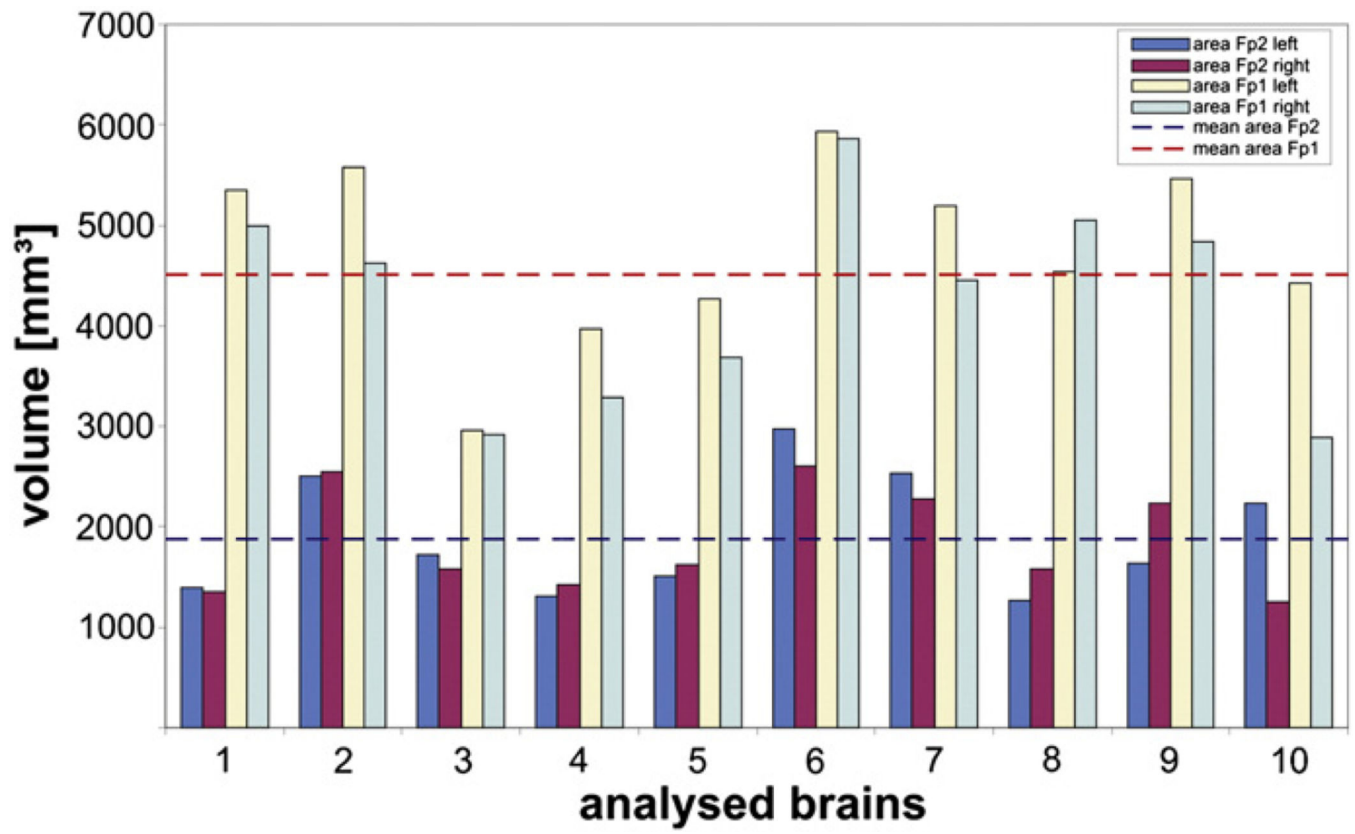


Fig. 9.
Comparison of single hemisphere volumes of Fp1 and Fp2.

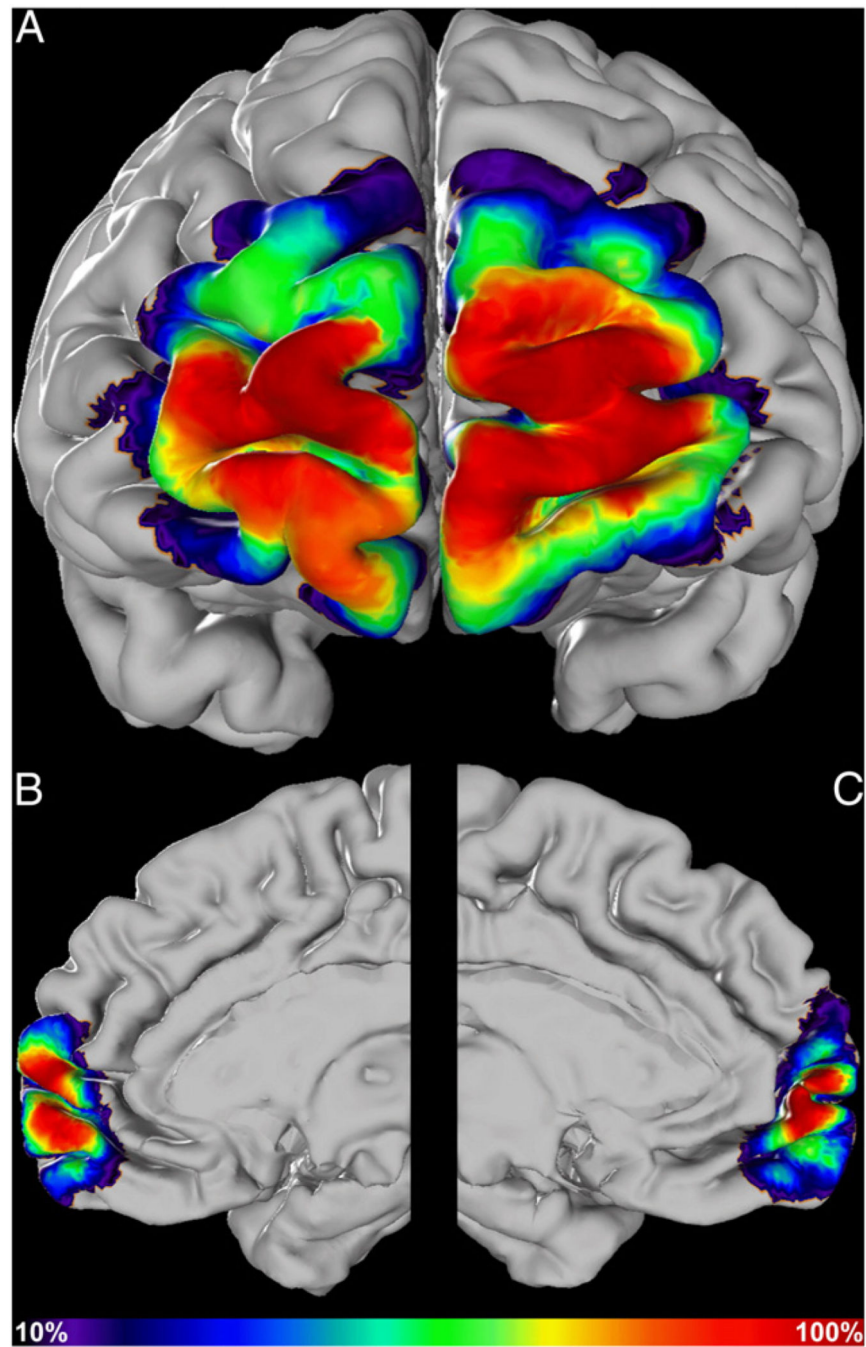


Fig. 10. Continuous probability maps of areas Fp1 and Fp2 registered to the MNI reference brain. Frontal A) and medial (left) B) (right) C) view onto the probabilistic maps of the delineated areas Fp1 A) and Fp2 B,C). Visualized as overlays on the MNI reference brain. The number of overlapping brains for each voxel is color coded; e.g., green means that approximately 6 of 10 brains overlapped in this voxel. The maps are visible at http://www.fz-juelich.de/inm/inm-1/jubrain_cytoviewer.

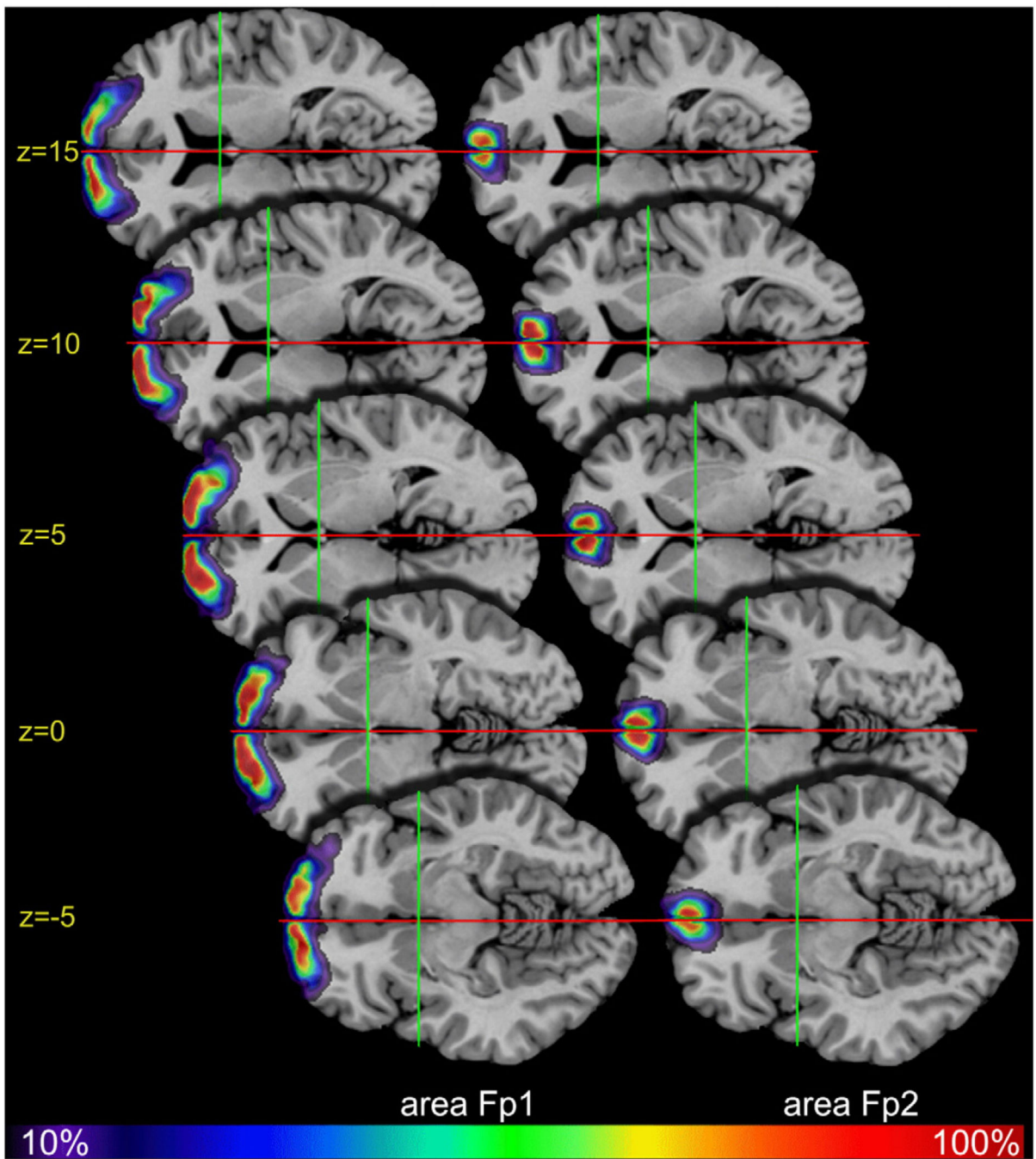


Fig. 11. Continuous probability maps of areas Fp1 and Fp2. Cytoarchitectonic probability map in anatomical MNI space (Amunts et al., 2005) of areas Fp1 and Fp2. The number of overlapping brains for each voxel is color coded. Yellow numbers indicate z-coordinates. Red and green lines cross in $x = 0$ and $y = 0$ coordinates of the different horizontal sections.

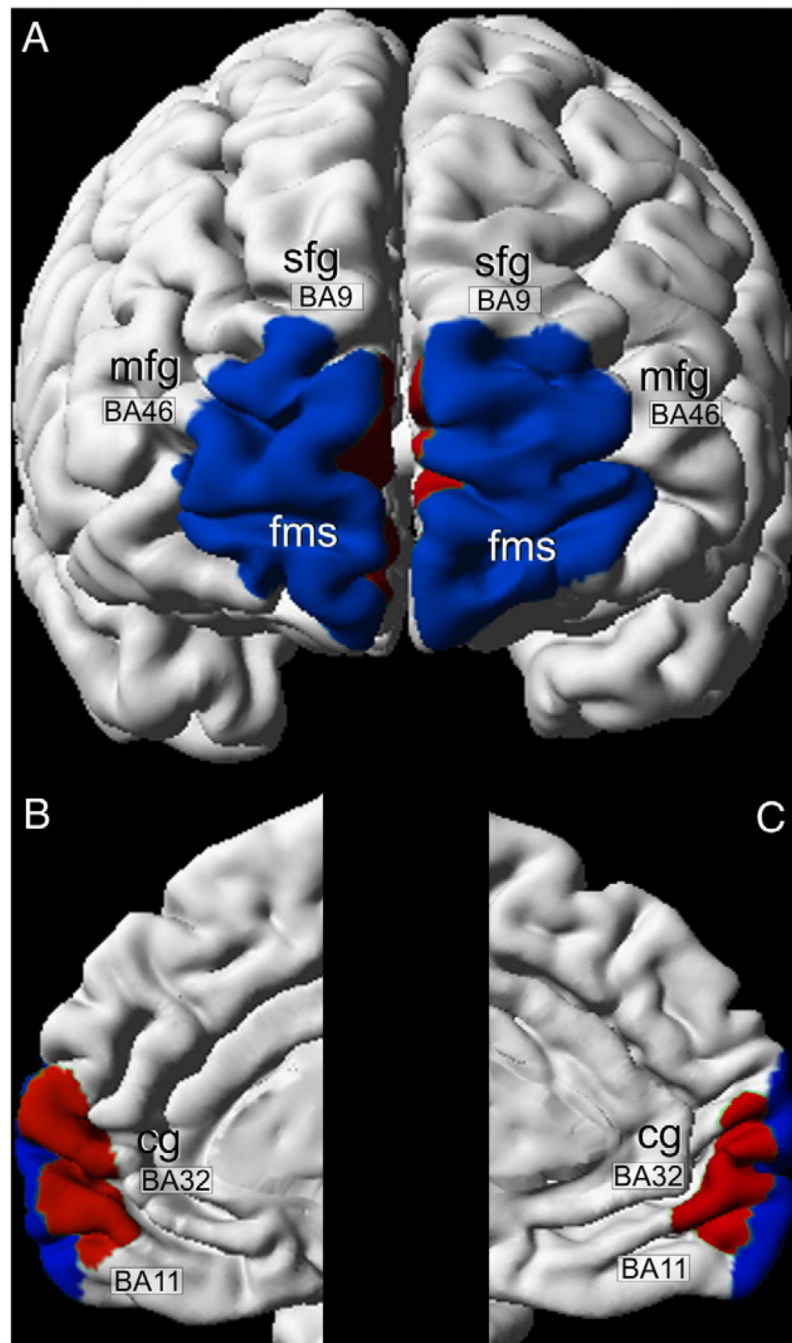


Fig. 12. Maximum probability map of areas Fp1 (blue) and Fp2 (red). Frontal A) and medial B,C) views of the maximum probability map displayed on the reconstructed MNI reference brain. Neighboring areas BA9, BA46, BA32 and BA11 were briefly outlined. (mfg = middle frontal gyrus, sfg = superior frontal gyrus, fms = frontomarginal sulcus, cg = cingulate gyrus).

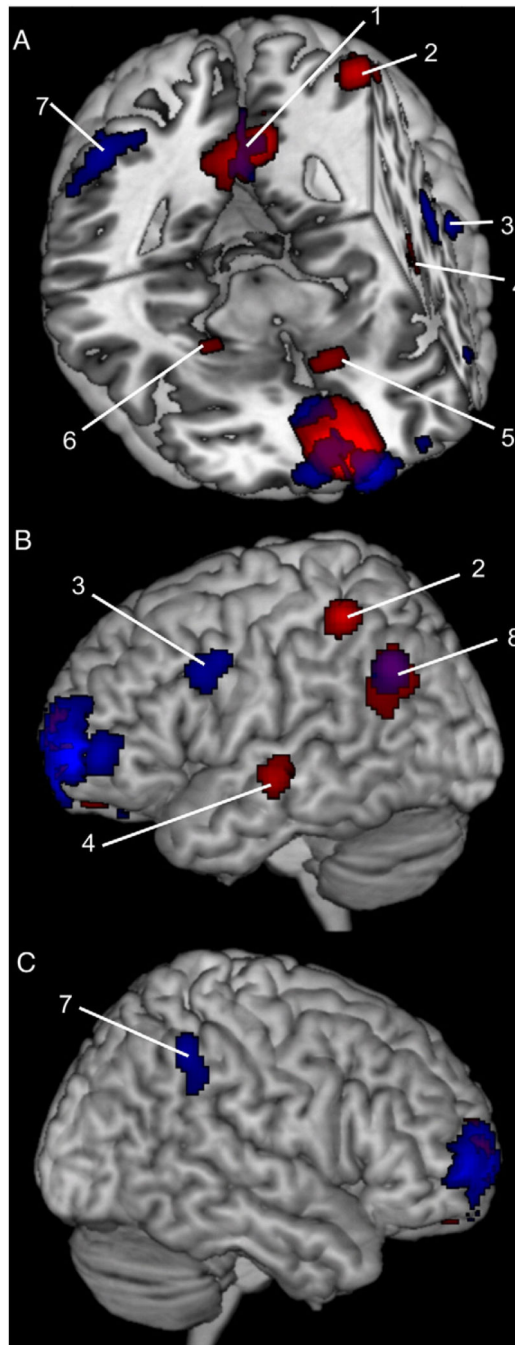


Fig. 13. 3D rendering of the contrast of significant co-activations cluster for area Fp2 and area Fp1. All results are displayed on the MNI single subject template. The results represent those regions that are significantly stronger co-activated with Fp1 and Fp2, respectively. Red spots: medial area Fp2 co-activations; blue spots: lateral area Fp1 co-activations. Cluster sizes and assigned cytoarchitectonic areas in Table 3. Macroanatomical locations: 1 posterior cingulate cortex; 2 left superior parietal lobule; 3 left precentral gyrus; 4 left middle

temporal gyrus; 5 left putamen; 6 right amygdala; 7 right inferior parietal lobule; 8 left angular gyrus.

Author Manuscript

Author Manuscript

Author Manuscript

Author Manuscript

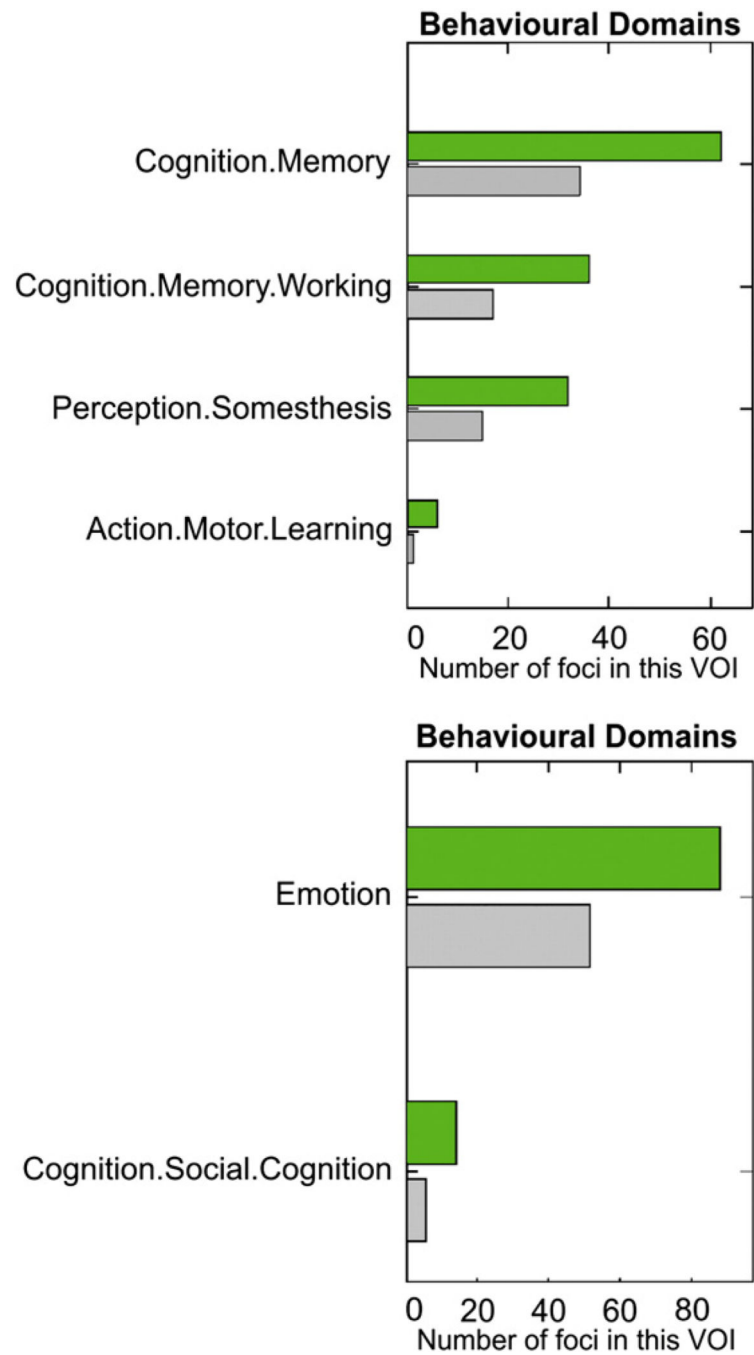


Fig. 14. Behavioural domains of significant clusters found based on a meta-analysis for area Fp1 (upper graph) and area Fp2 (lower graph). Functional characterization by behavioral domain metadata based on the BrainMap database classifications (www.brainmap.org, (Fox and Lancaster, 2002)). Green bar: number of foci found with the meta-analyses; grey bar: number of expected hits by chance.

Table 1

Sample of post mortem brains used for cytoarchitectonic analysis.

Brain number	Gender	Age [years]	Cause of death	Cutting plane
pm14	Female	86	Cardiorespiratory insufficiency	Coronal
pm18	Female	75	Cardiorespiratory insufficiency	Horizontal
pm 24	Female	72	Heart infarction	Horizontal
pm 23	Female	63	Bronchial carcinoma	Horizontal
pm 17	Female	50	Heart infarction	Horizontal
pm 22	Male	85	Ileus	Horizontal
pm 16	Male	63	Accident	Horizontal
pm 6	Male	54	Heart infarction	Coronal
pm 15	Male	54	Gunshot injury	Horizontal
pm 21	Male	30	Bronchopneumonia and Morbus Hodgkin	Coronal

Author Manuscript

Author Manuscript

Author Manuscript

Author Manuscript

Table 2

Cytoarchitectonic features of areas Fp1, Fp2 and surrounding cytoarchitectonic areas.

Fp1	Sharp border between layers I, II, and III Dense layers II and III (deep part) Considerably larger pyramids in deeper than in upper layer III Broader layer IV than Fp2
Fp2	Sharp border between layers I, II, and III Low cell density in layer II Larger pyramids in deeper than in upper layer III Medium sized pyramidal cells in upper layer V
BA9	No sharp border between layers I, II, and III Medium sized pyramidal cells in layer III Prominent layers II and IV, but narrower than in Fp1
BA11	Thinner cortex than in Fp1 and Fp2 Thinner layer IV than in Fp1 and Fp2
BA46	Dense layer II Homogenous layer V Sharp border between layer VI and white matter
BA32	Broad and dense layer II Larger pyramids in deeper than in upper layer III Dysgranular Upper layer V more cell dense than lower layer V

Table 3

Dataset of volumetric analyses of area frontopolaris. Mean volumes of area frontopolaris (area Fp1 and Fp2 together) of grouped hemispheres and genders were calculated from the shrinkage corrected volumes of the 10 analyzed brains. (SD = standard deviation; p = contrast estimate of the pair wise permutation tests (significant differences if $p < 0.05$)).

Mean volume per hemisphere (n = 10) [mm ³]	Mean	SD	p
Male	6922.65	1342.90	0.08
Female	5858.53	1193.25	
Left (male and female)	7235.00	1165.90	0.36
Right (male and female)	6610.29	1566.64	
Volume proportion of area frontopolaris per hemisphere compared to the entire brain volume(n = 10) (volume area frontopolaris/brain volume)[%]			
Male	0.50	0.08	0.42
Female	0.47	0.09	
Left (male and female)	0.51	0.07	0.27
Right (male and female)	0.47	0.09	

Table 4

Co-activation cluster for the medial and lateral part of area 10. Cytoarchitectonic areas assigned according to Caspers et al. (2008) (inferior parietal cortex (IPC) (PGa, PFm)), Amunts et al. (1999) (left precentral gyrus (Area 44)), Geyer (2004) (right mid-orbitofrontal gyrus (area 6)), Grefkes et al. (2001) (left superior parietal lobule (SPL) (left area 2)), Amunts et al. (2005) (right laterobasal group of the amygdala (Amyg (LB))). All peaks are assigned to the most probable brain areas, see SPM Anatomy Toolbox (Eickhoff et al., 2005).

Macroanatomical location	Cytoarchitectonic areas	Cluster size [Voxel]	MINI coordinates x y z
<i>co-activations Fp2</i>			
Left Middle Cingulate Cortex		1194	-8 -48 34
Right Posterior Cingulate Cortex			2 -50 30
Left Precuneus			-4 -56 20
Right Middle Cingulate Cortex			12 -40 34
Left Angular Gyrus	left IPC (PGa) [59.5%] left IPC (PGp) [32.2%]	402	-50 -62 38
Left Putamen		205	-22 6 4
Left Caudate Nucleus			-10 12 -8
Left Superior Parietal Lobule	left area 2 [68%] left SPL (7PC) [16.3]	155	-40 -44 56
Left Middle Temporal Gyrus		140	-54 -18 -6
Right Amygdala	right Amyg (LB) [60.3%]	134	28 -6 -20
Right Hippocampus	right Hipp (CA) [21.5%]		
<i>co-activations Fp1</i>			
Left Precuneus		307	-2 -58 36
Left Posterior Cingulate Cortex			-2 -50 22
Left Middle Cingulate Cortex			-8 -48 34
Right Middle Cingulate Cortex			6 -40 36
Left Angular Gyrus	Left IPC (PGa) [71%] left IPC (PGp) [25.9]	220	-48 -62 36
Left Precentral Gyrus	left Area 44 [37.4%]	195	-50 10 34
Right Inferior Parietal Lobule	right IPC (PFm) [60.5%] right hIP2 [13.5%]	184	46 -48 48

Author Manuscript

Author Manuscript

Author Manuscript

Author Manuscript

Macroanatomical location	Cytoarchitectonic areas	Cluster size [Voxel]	MNI coordinates		
			x	y	z
Right Mid Orbital Gyrus		167	4	32	-14
Left Rectal Gyrus			-4	38	-20
Left SMA	Left Area 6 [12.5%]	147	-2	20	52
Left Middle Cingulate Cortex			-4	28	32